

## Chapter I.11

### Linear particle accelerators

*David Alesini*

INFN, Laboratori Nazionali di Frascati, Italy

---

A linac (linear accelerator) is a system that allows to accelerate charged particles through a linear trajectory by electromagnetic fields. This kind of accelerator finds several applications in fundamental research and industry. The main devices used to accelerate the particle beam will be introduced in the first part of the paper, while in the second part, the fundamentals of the longitudinal and transverse beam dynamics will be highlighted. A short paragraph is finally dedicated to radiofrequency quadrupoles (RFQ).

---

#### I.11.1 Introduction

A linear accelerator (linac) is a device that accelerates charged particles (electrons, protons, ions) along a straight trajectory [1,2] The main advantage of linacs is their capability to produce high-energy, high-intensity charged particle beams of excellent quality in terms of beam emittance and energy spread. These devices find applications in different fields such as research, healthcare and industry [3–8] The acceleration can be obtained with constant (DC) or time-varying electric fields. In the second case, we can have two types of linacs: Radio Frequency (RF) and induction. In this proceeding we will refer to RF linacs in which the particle acceleration is obtained by electromagnetic fields confined in resonant cavities fed by sinusoidal time-varying power sources. The design and the structure of a linac depend on the type of accelerated particles (e.g. electrons, protons or ions) and on the required final beam parameters in terms of energy, energy spread, emittance and current. In the design and in the choice of the technology, several constraints have also to be taken into account such as cost, available footprint and power consumption. The main advantages [9] of linacs with respect to other possible particle accelerators (as synchrotrons or cyclotrons) are the fact that they can handle high peak current beams, they can run with high duty-cycle and they exhibit low synchrotron radiation losses (in the case of light particle acceleration as electron or positrons). On the contrary, the main drawback is the fact that they require a large number of cavities to reach a desired energy, since the beam passes only once in the accelerating structures. Moreover, synchrotron radiation damping (in the case of light particles) cannot be used to reduce the beam emittance without adopting complicated schemes. Linacs are mainly used in fundamental physics research as injectors for synchrotrons and storage rings, free electron lasers and injectors for colliders. They also find a large number of medical and industrial applications for cancer therapy, X-rays generation, material treatment, food irradiation and ion implantation. A linac conceptual

---

This chapter should be cited as: Linear particle accelerator, D. Alesini, DOI: [10.23730/CYRSP-2024-003.479](https://doi.org/10.23730/CYRSP-2024-003.479), in: Proceedings of the Joint Universities Accelerator School (JUAS): Courses and exercises, E. Métral (ed.), CERN Yellow Reports: School Proceedings, CERN-2024-003, DOI: [10.23730/CYRSP-2024-003](https://doi.org/10.23730/CYRSP-2024-003), p. 479.  
© CERN, 2024. Published by CERN under the [Creative Commons Attribution 4.0 license](https://creativecommons.org/licenses/by/4.0/).

scheme, where its technology complexity can be also assessed, is shown in Fig. I.11.1. Particles are generated and pre-accelerated in the injector, and then accelerated by accelerating structures and focused by magnetic elements (quadrupoles and solenoids). Beam trajectory and dimensions along the linac are measured by different types of diagnostic devices (striplines, cavity beam position monitors and beam screens) depending on the particle beam and energy. In the figure, the control, cooling and vacuum systems, the RF distribution and RF power sources are also indicated.

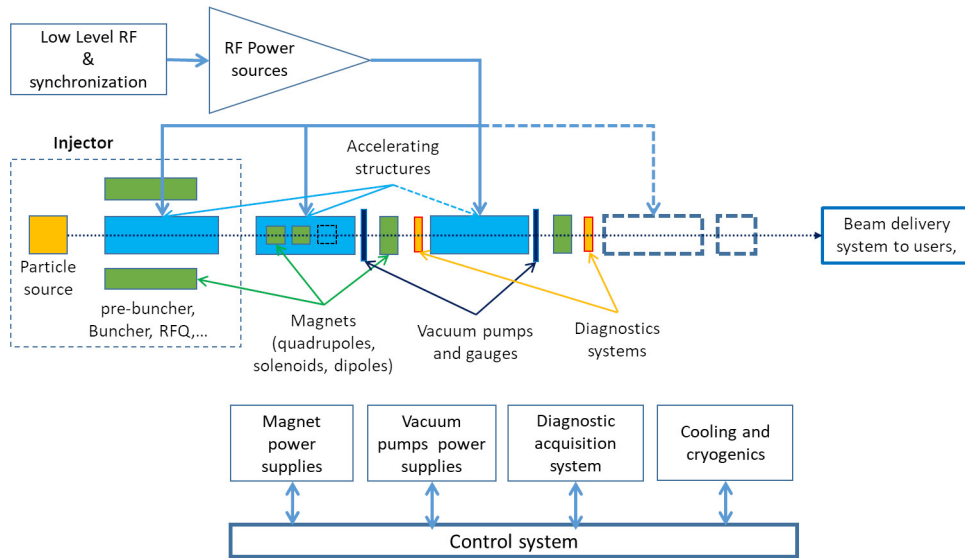


**Fig. I.11.1:** Schematic layout of a linac [10].

### I.11.2 Acceleration process: particle velocity and energy

The first historical linear accelerator was conceived by the Nobel prize Wilhelm Conrad Röntgen (1901). It consisted in a vacuum tube containing a cathode connected to the negative pole of a DC voltage generator of few kV. Electrons emitted by the heated cathode (by thermionic emission) were accelerated while flowing to another electrode connected to the positive generator pole (anode). Collisions between the energetic electrons and the anode produced X-rays and gave the possibility to do the first radiography. In modern electrostatic accelerators high voltage is shared between a set of electrodes creating an accelerating field between them. This type of accelerator is better known as the Cockcroft-Walton accelerator [11]. Its main limitation in term of achievable energy is due to the fact that all partial accelerating voltages add up and at some point insulation problems or discharges occur, thus limiting the maximum achievable voltage to a few tens of MV. Electrostatic accelerators are still used for several applications as X-ray generation, material analysis, or ion implantation. The simple scheme of a DC acceleration process between two electrodes is reported in Fig. I.11.2. Considering the energy-momentum relation and the Lorentz force we can easily write the following relations

$$E^2 = E_0^2 + p^2 c^2 \Rightarrow 2E dE = 2p dp c^2 \Rightarrow dE = v \frac{mc^2}{E} dp \Rightarrow dE = v dp \quad , \quad (\text{I.11.1})$$

$$\frac{dp}{dt} = q E_z \underbrace{\Rightarrow}_{z=vt} v \frac{dp}{dz} = q E_z \Rightarrow \frac{dE}{dz} = q E_z \text{ (and also } \frac{dW}{dz} = q E_z) \quad , \quad (\text{I.11.2})$$

where  $E_0 (= m_0 c^2)$  is the particle rest energy,  $E$  is the total energy,  $m_0$  is the rest mass,  $m$  is the relativistic mass,  $v$  is the particle velocity,  $p (= mv)$  is the particle momentum,  $W = E - E_0$  is the kinetic energy and  $E_z$  is the accelerating field. In Eq. (I.11.2),  $\frac{dE}{dz}$  is the rate of energy gain per unit length and it is proportional to the accelerating field  $E_z$ . Integrating Eq. (I.11.2) on the accelerating gap we obtain the energy gain per electrode pair  $\Delta E$

$$\Delta E = \int_{\text{gap}} \frac{dE}{dz} dz = \int_{\text{gap}} q E_z dz \Rightarrow \Delta E = q \Delta V \quad . \quad (\text{I.11.3})$$

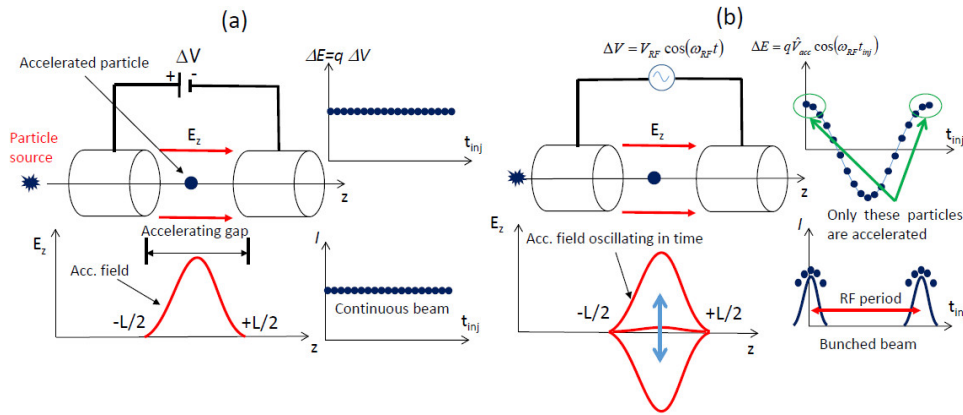


**Fig. I.11.2:** Scheme of acceleration processes between two electrodes: (a) electrostatic acceleration; (b) RF acceleration [10].

If now we consider the relativistic factors  $\beta = v/c$  and  $\gamma = E/E_0$  we can write

$$\beta = \sqrt{1 - \frac{1}{\gamma^2}} = \sqrt{1 - \left(\frac{E_0}{E}\right)^2} = \sqrt{1 - \left(\frac{E_0}{E_0 + W}\right)^2} \quad . \quad (\text{I.11.4})$$

The behavior of  $\beta$  and  $\gamma$  as a function of the kinetic energy is given in Fig. I.11.3 for an electron and a proton. From the plot it is evident that light particles (electrons) are practically fully relativistic ( $\beta \simeq 1, \gamma \gg 1$ ) at relatively low energies (above  $\sim 10$  MeV) and reach a constant velocity ( $\sim c$ ). Thus, for this type of particles, the acceleration process occurs at constant velocity. On the contrary heavy particles (protons and ions) are typically weakly relativistic and reach a constant velocity only at very high energies. This means that their velocity changes during the acceleration process. As illustrated in the following, the possible velocity change during acceleration generates important differences in the accelerating structures design and beam dynamics between light and heavy particles.

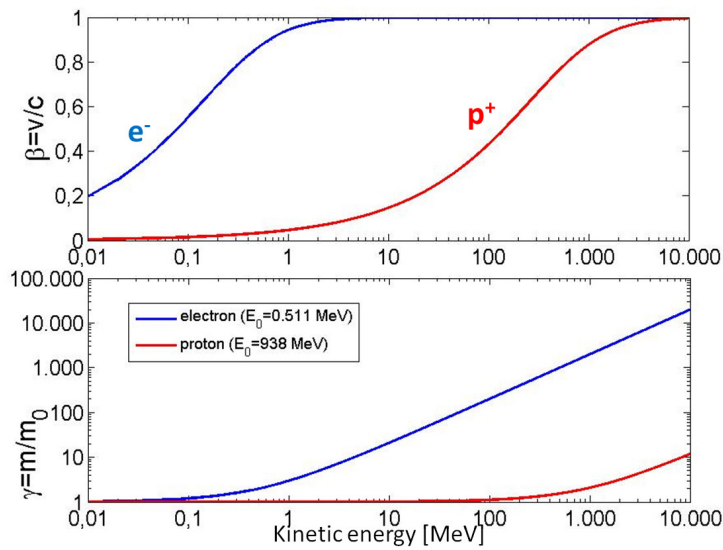


**Fig. I.11.3:**  $\beta$  (top) and  $\gamma$  (bottom) as a function of the kinetic energy for an electron (blue) and a proton (red) [10].

### I.11.3 Radiofrequency accelerators: the Widerøe linac

In the late 1920's propositions were made by Ising (1924) and implemented by Widerøe (1927) to overcome the limitation of electrostatic devices in terms of reachable energy [12–14]. The scheme they proposed is illustrated in Fig. I.11.4. An AC voltage generator feeds, alternately, a series of electrodes in

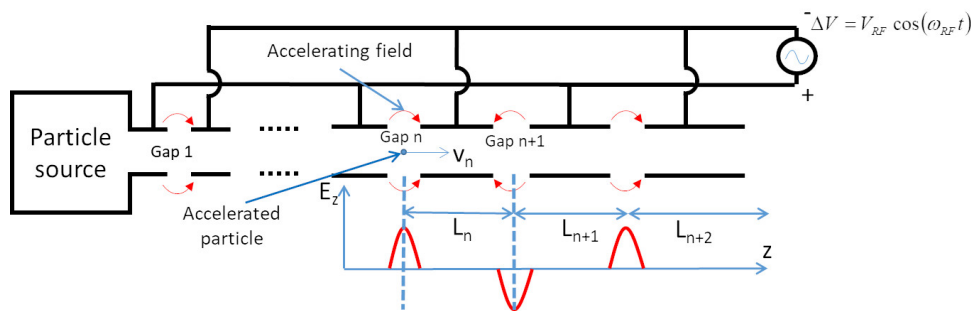


**Fig. I.11.4:** Conceptual scheme of a Widerøe linac [10].

such a way that particles that do not experience any force while travelling inside the tubes (Drift Tubes) are accelerated across the gaps. In particular, this last statement is true if the drift tube length (or, equivalently, the distances between the centers of the accelerating gaps  $L_n$ ) increases with the particle velocity during the acceleration, such that the time of flight between gaps is kept constant and equal to half of the RF period. If this condition is satisfied, the particles are subject to a synchronous accelerating voltage and experience an energy gain of  $\Delta E = q \Delta V$  at each gap.

In this type of structures, called drift tube linac (DTL), a single RF generator can be used, in principle, to indefinitely accelerate the beam, avoiding the breakdown limitations that affect the electrostatic accelerators. The Widerøe linac was the first RF linac. As illustrated in Fig. I.11.2(b), a RF acceleration

process does not allow to accelerate a continuous particle beam but the beam needs to be “bunched” with a distance between bunches exactly equal to the RF period.

Let us now consider the acceleration between a pair of two electrodes. The behavior of the accelerating electric field and voltage are given by the following relations

$$\begin{cases} E_z(z, t) &= E_{\text{RF}}(z) \cos(\omega_{\text{RF}} t) \\ \Delta V &= V_{\text{RF}} \cos(\omega_{\text{RF}} t) \\ \omega_{\text{RF}} &= 2\pi f_{\text{RF}} = \frac{2\pi}{T_{\text{RF}}} \\ V_{\text{RF}} &= \int_{\text{gap}} E_{\text{RF}}(z) dz \end{cases} \quad . \quad (\text{I.11.5})$$

The energy gain per electrode (supposing a symmetric accelerating field with respect to  $z = 0$ ) is given by

$$\begin{aligned} \Delta E &= q \int_{\text{gap}} E_z(z, t) dz = q \int_{-L/2}^{+L/2} E_{\text{RF}}(z) \cos\left(\omega_{\text{RF}} \frac{z}{v} + \varphi_{\text{inj}}\right) dz \\ &= q \underbrace{\int_{\text{gap}} E_{\text{RF}}(z) dz}_{V_{\text{RF}}} \underbrace{\frac{\int_{\text{gap}} E_{\text{RF}}(z) \cos(\omega_{\text{RF}} \frac{z}{v}) dz}{\int_{\text{gap}} E_{\text{RF}}(z) dz}}_T \cos(\varphi_{\text{inj}}) = q \underbrace{\frac{\widehat{V}_{\text{acc}}}{V_{\text{RF}} T}}_{V_{\text{acc}}} \cos(\varphi_{\text{inj}}) \quad , \quad (\text{I.11.6}) \end{aligned}$$

where  $\varphi_{\text{inj}}$  is the injection phase of a generic particle and  $T$  is the “transit time factor” (which is always smaller than 1). It takes into account the fact that the RF voltage is oscillating in time while the beam is traversing the gap and that the effective peak accelerating voltage ( $\widehat{V}_{\text{acc}}$ ) is in fact equal to the RF voltage ( $V_{\text{RF}}$ ) multiplied by this factor.  $\widehat{E}_{\text{acc}} = \frac{\widehat{V}_{\text{acc}}}{L}$  [V/m] is the average accelerating field in the gap and  $E_{\text{acc}} = \frac{V_{\text{acc}}}{L}$  [V/m] is the average accelerating field seen by the particle. If we consider a Widerøe structure, the energy gain, at each gap, is equal to  $\Delta E_n = q V_{\text{acc}}$  while the particle velocity increases accordingly to Eq. (I.11.4). In order to be synchronous with the accelerating field at the center of each gap, the time of flight ( $t_n$ ) between gaps has to be related to the generator RF period ( $T_{\text{RF}}$ ) and RF wavelength ( $\lambda_{\text{RF}}$ ) by the following relation

$$t_n = \frac{L_n}{\bar{v}_n} = \frac{T_{\text{RF}}}{2} \quad \Rightarrow \quad L_n = \frac{1}{2} \bar{v}_n T_{\text{RF}} = \frac{1}{2} \bar{\beta}_n \underbrace{c T_{\text{RF}}}_{\lambda_{\text{RF}}} \quad , \quad (\text{I.11.7})$$

where  $\bar{v}_n$  is the average particle velocity between the gap  $n$  and  $n + 1$ . Then, the distance between the centers of two consecutive gaps has to be increased as follows

$$L_n = \frac{1}{2} \bar{\beta}_n \lambda_{\text{RF}} \quad . \quad (\text{I.11.8})$$

The energy gain per unit length is then given by

$$\frac{\Delta E}{\Delta L} = \frac{q V_{\text{acc}}}{L_n} = \frac{2 q V_{\text{acc}}}{\lambda_{\text{RF}} \bar{\beta}_n} \quad . \quad (\text{I.11.9})$$

### I.11.4 RF cavities

There are two important consequences of Eq. (I.11.8) obtained in the previous paragraph. First of all, the condition  $L_n \ll \lambda_{\text{RF}}$  (necessary to model the tube as an equipotential region) requires  $\beta_n \ll 1$ . This implies that the Widerøe acceleration technique cannot be applied to relativistic particles. Moreover, when the particles velocity increases the drift tube gets longer, reducing the acceleration efficiency (energy gain per unit length  $\frac{\Delta E}{\Delta L}$ ). The average accelerating field ( $E_{\text{acc}}$ ) increase pushes towards the use of small  $\lambda_{\text{RF}}$  (higher frequencies), but the concept of equipotential drift tubes cannot be applied at small  $\lambda_{\text{RF}}$  and the power lost by free space radiation increases proportionally to the RF frequency. All previous considerations combined with the fact that high-frequency, high-power RF sources became available only after World War II (thanks to the perfectioning of radar technology for military purposes), pushed to develop more efficient accelerating structures than simple drift tubes. In order to avoid electromagnetic (e.m.) radiation processes and to allow the use of high-frequency sources, the accelerating system had to be enclosed in a metallic volume: a RF cavity. In a RF cavity, the e.m. field has a particular spatial configuration (resonant mode) whose components, including the accelerating field  $E_z$ , oscillate at a specific frequency (called resonant frequency) characteristic of the mode. The mode is excited by the RF generator that is coupled to the cavity through waveguides, coaxial cable antennas or loops. The resonant modes are called Standing Wave (SW) modes since they have a fixed spatial configuration that oscillates in time. The spatial and temporal field profiles in a cavity have to be computed (analytically or numerically) by solving the Maxwell equations with the proper boundary conditions [15, 16]. For a SW cavity the accelerating field on the  $z$ -axis can be written, in a general form, as

$$E_z(z, t) = E_{\text{RF}}(z) \cos(\underbrace{2\pi f_{\text{RF}} t}_{\omega_{\text{RF}}} + \varphi) = \Re[\tilde{E}_z(z) e^{j\omega_{\text{RF}} t}] \quad , \quad (\text{I.11.10})$$

where  $f_{\text{RF}}$  is the excitation frequency of the generator equal to (or close to) the resonant frequency of the cavity,  $\omega_{\text{RF}}$  is the angular excitation frequency,  $E_{\text{RF}}$  (or the phasor  $\tilde{E}_z(z)$ ) is a real (complex) function related to the spatial configuration of the mode. RF linacs use different types of cavities depending on the species and energy range of particles to be accelerated, as described in the following paragraphs.

### I.11.5 Alvarez structures

The Alvarez structures [17], reproduced in Fig. I.11.5, can be described as special DTLs in which the electrodes are part of a resonant macrostructure. They work in the “0-mode”, since the accelerating field at a given time has the same phase in each gap. The Widerøe structures, on the contrary, work in the “ $\pi$ -mode”, i.e. the accelerating field in consecutive gaps has opposite sign. They are used for protons and ions in the range of  $\beta=0.05$ -0.5. They typically operate at  $f_{\text{RF}} = 50$ –400 MHz,  $\lambda_{\text{RF}} = 6$ –0.7 m in the 1–100 MeV energy range. Usually, they are simply called DTL (instead of the Widerøe structures that are not used anymore). As for the Widerøe structure, also in the Alvarez linac the accelerating field is concentrated between gaps and the beam crosses the drift tubes when the electric field is decelerating. The drift tubes are suspended by stems and quadrupole magnets (for transverse focusing) can fit inside them. To maintain the synchronism between the beam and the accelerating field at each gap, the distance

between the accelerating gaps  $L_n$  has to be varied according to the formula

$$L_n = \bar{\beta}_n \lambda_{\text{RF}} \quad . \quad (\text{I.11.11})$$

To maintain the synchronism, in principle, both the gap and the drift tube length can be varied. A generally applied criterion is to maintain a constant transit time factor according to Eq. (I.11.6). Some examples of Alvarez structures can be found in the CERN Linac4 [18] operating at 352 MHz frequency with 3 resonators tanks of  $\sim 500$  mm diameter, 19 m long, 120 drift tubes, that accelerate protons from 3 MeV to 50 MeV ( $\beta = 0.08$  to 0.31). In this case the distance between gaps varies from 68 mm to 264 mm.

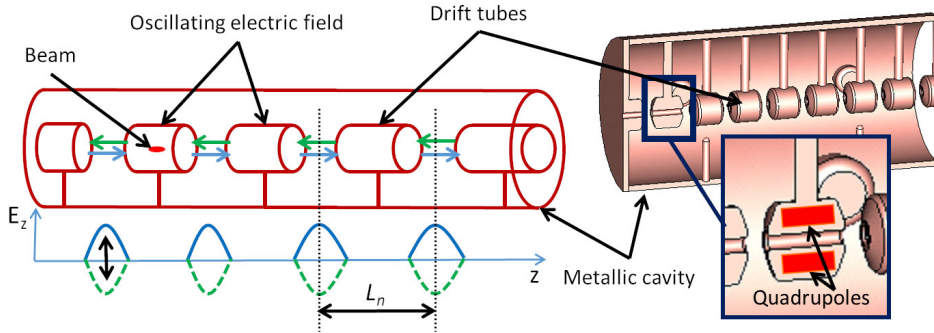


**Fig. I.11.5:** Schematic view of the Alvarez structure (drift tube linac) [10].

### I.11.6 High $\beta$ cavities: cylindrical standing wave structures

When the  $\beta$  of the particles increases ( $> 0.5$ ) one has to use higher RF frequencies ( $> 400\text{--}500$  MHz) to increase the accelerating gradient per unit length. It is possible to demonstrate that DTL structures become less efficient (effective accelerating voltage per unit length for a given input power) for such values of  $\beta$ . In this range of frequencies, cylindrical single or multiple cavities working in the  $\text{TM}_{010}$ -like mode are used. For a pure cylindrical structure (usually called a “pillbox cavity”) the first accelerating mode (i.e. the mode with non-zero longitudinal electric field on axis) is the  $\text{TM}_{010}$  mode. It has a well-known analytical solution (obtained solving Maxwell’s equations), and its spatial configuration in the case of a pure cylindrical cavity is given in Fig. I.11.6(a). For this mode the electric field has only a longitudinal component, while the magnetic one is purely azimuthal. The corresponding complex phasors are given by [15]

$$\begin{cases} \tilde{E}_z &= A J_0 \left( p_{01} \frac{r}{a} \right) \\ \tilde{H}_\theta &= -j A \frac{1}{Z_0} J'_0 \left( p_{01} \frac{r}{a} \right) \end{cases} , \quad (\text{I.11.12})$$

where  $a$  is the cavity radius,  $A$  is the mode amplitude and  $p_{01}$  ( $= 2.405$ ) is the first zero of the Bessel function  $J_0$ . The resonant frequency of this mode is given by  $f_{\text{res}} = \frac{p_{01}c}{2\pi a}$ .

The geometry of real cylindrical cavities is somewhat different from that of a pillbox. In fact, one must also consider the perturbation introduced by the beam pipe, the power couplers to the RF generators and any antenna or pick-up used to monitor the accelerating field inside the cavity. For this reason, the actual accelerating mode is called the  $\text{TM}_{010}$ -like mode. Real cavities and their couplers to

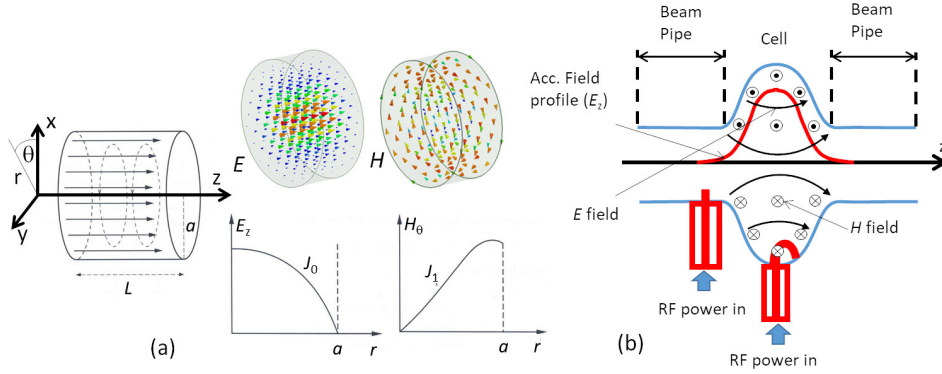


**Fig. I.11.6:** (a) Ideal pillbox cavity and e.m. field configuration; (b) Sketch of a real cavity operating in the  $TM_{010}$ -like mode with two types of coaxial couplers (antenna and loop) [10].

the RF generators are designed using numerical codes that solve the Maxwell equations with the proper boundary conditions. A sketch of a cavity fed through a loop or a coaxial probe to an external generator is given in Fig. I.11.6(b), where the electric and magnetic field lines and the longitudinal electric field profile on the axis are also shown. Details of the coupler design can be found in Ref. [19].

### I.11.6.1 SW cavity parameters: shunt impedance and quality factor

For a SW cavity the first figure of merit is the shunt impedance defined in Refs. [1, 2, 15, 20]

$$R = \frac{\hat{V}_{\text{acc}}^2}{P_{\text{diss}}} \quad [\Omega] \quad , \quad (\text{I.11.13})$$

where  $\hat{V}_{\text{acc}}$  is the peak accelerating voltage (i.e. the maximum energy gain per unit charge) for a given dissipated power into the cavity ( $P_{\text{diss}}$ ).  $\hat{V}_{\text{acc}}$  is obtained by integrating the time-varying accelerating field sampled by the charge along the trajectory

$$\hat{V}_{\text{acc}} = \left| \int_{\text{cavity}} \tilde{E}_z(z) e^{j\omega_{\text{RF}} \frac{z}{v}} dz \right| \quad , \quad (\text{I.11.14})$$

with  $v$  the particle velocity, while the total average dissipated power  $P_{\text{diss}}$  is given by the integral of the power density on the cavity wall

$$P_{\text{diss}} = \int_{\text{cavity wall}} \underbrace{\frac{1}{2} R_s |\tilde{H}_{\text{tan}}|^2}_{\text{power density}} dS \quad , \quad (\text{I.11.15})$$

where  $\tilde{H}_{\text{tan}}$  is the tangential magnetic field component on the surface of the cavity. The shunt impedance qualifies the efficiency of the cavity: the higher its value, the larger the achievable accelerating voltage for a given dissipated power. As an example, at 1 GHz for a normal conducting (NC) copper cavity a typical shunt impedance of the order of 2 M $\Omega$  can be obtained, while a superconducting (SC) cavity, at the same frequency, can reach values of the order of 1 T $\Omega$ , due to the extremely lower dissipated power.

It is also useful to refer to the following quantity the shunt impedance per unit length

$$r = \frac{R}{L} = \frac{\left(\frac{\hat{V}_{\text{acc}}}{L}\right)^2}{\frac{P_{\text{diss}}}{L}} = \frac{\hat{E}_{\text{acc}}^2}{p_{\text{diss}}} \quad [\Omega/\text{m}] \quad , \quad (\text{I.11.16})$$

where  $L$  is the cavity length,  $\hat{E}_{\text{acc}}$  the average accelerating field and  $p_{\text{diss}}$  the dissipated power per unit length. The quality factor of the accelerating mode is then defined by the ratio of the cavity stored energy ( $W$ ) and the dissipated power on the cavity walls

$$Q_0 = \omega_{\text{RF}} \frac{W}{P_{\text{diss}}} \quad , \quad (\text{I.11.17})$$

where the total energy ( $W$ ) stored in the cavity is given by integrating the expression for the energy density in the cavity

$$W = \int_{\text{cavity volume}} \underbrace{\left( \frac{1}{4} \epsilon |\vec{E}|^2 + \frac{1}{4} \mu |\vec{H}|^2 \right)}_{\text{energy density}} dV \quad . \quad (\text{I.11.18})$$

For a NC cavity operating at 1 GHz the quality factor is of the order of  $10^4$  while, for an SC cavity, values of the order  $10^9$  to  $10^{10}$  can be achieved. It can be easily demonstrated that the ratio  $R/Q$  is a pure geometrical factor and it does not depend upon the cavity wall conductivity or operating frequency. This is the reason why it is always taken as a geometric design qualification parameter. The  $R/Q$  of a single cell is of the order of 100.

### I.11.6.2 Standing wave cavity equivalent circuit

The quantities described above play crucial roles in the evaluation of the cavity performances. Let us consider a cavity powered by a source (klystron) at a constant frequency  $f_{\text{RF}}$  in CW and at a fixed power ( $P_{\text{in}}$ ) as shown in Fig. I.11.7. It can be demonstrated that the equivalent circuit of the SW cavity is that of a parallel RLC resonant circuit where the resistance  $R$  is exactly the shunt impedance of the cavity, and the quality factor is the quality factor of the RLC circuit. The transformer models the coupling between the waveguide and the cavity. With simple calculations, it is easy to demonstrate that the maximum accelerating voltage  $\hat{V}_{\text{acc}}$  for a given input power  $P_{\text{in}}$  is given by

$$\hat{V}_{\text{acc}} = \frac{\frac{2\sqrt{\beta}}{1+\beta}}{\sqrt{1 + (Q_L \delta)^2}} \sqrt{R P_{\text{in}}} \quad , \quad (\text{I.11.19})$$

where  $\beta$  is the generator–cavity coupling coefficient [3],  $Q_L = \frac{Q_0}{(1+\beta)}$  is the loaded quality factor and  $\delta = \left( \frac{f_{\text{RF}}}{f_{\text{res}}} - \frac{f_{\text{res}}}{f_{\text{RF}}} \right)$ . The dissipated power into the cavity is given by

$$P_{\text{diss}} = \frac{\frac{4\beta}{(1+\beta)^2}}{1 + (Q_L \delta)^2} P_{\text{in}} \quad . \quad (\text{I.11.20})$$

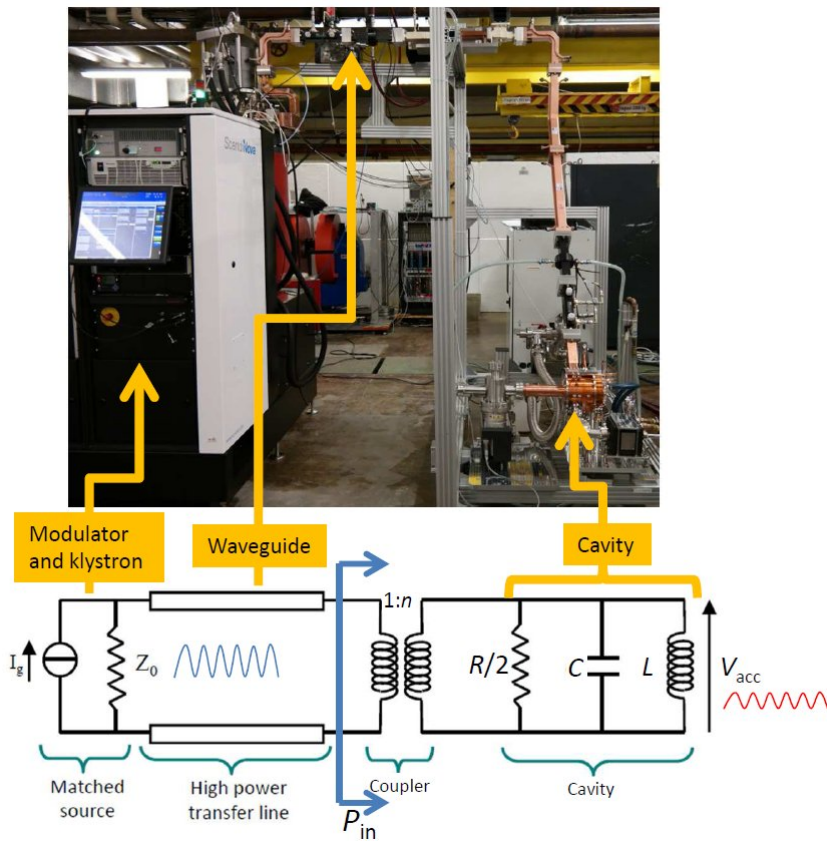


**Fig. I.11.7:** Equivalent circuit of a cavity fed by a generator [10].

The plot of the accelerating voltage as a function of the excitation frequency is given in Fig. I.11.8 for three different values of the cavity quality factor supposing  $P_{\text{in}} = 1 \text{ MW}$ ,  $\frac{R}{Q} = 100$  and  $\beta = 1$  (critical coupling), and  $f_{\text{res}} = 1 \text{ GHz}$ . From previous formulas we easily see that, at the resonant frequency and in the case  $\beta = 1$ , we have

$$\hat{V}_{\text{acc}} = \sqrt{R P_{\text{in}}} = \sqrt{\left(\frac{R}{Q}\right) Q_0 P_{\text{in}}} \quad . \quad (\text{I.11.21})$$

This means that, for a given cavity, the accelerating voltage is proportional to  $\sqrt{Q_0}$ .

On the other hand, the bandwidth of the resonance, defined as the  $\delta$ -frequency interval corresponding to the points with an average dissipated power in the cavity of a factor of two lower than the dissipated power at resonance, is inversely proportional to the cavity quality factor according to the formula

$$\frac{\Delta f_{\text{RF}|3\text{dB}}}{f_{\text{res}}} = \frac{1}{Q_L} \quad \Rightarrow \quad \begin{cases} \Delta f_{\text{RF}|3\text{dB}|_{\text{NC}}} \simeq 100 \text{ kHz} \\ \Delta f_{\text{RF}|3\text{dB}|_{\text{SC}}} < 1 \text{ Hz} \end{cases} \quad . \quad (\text{I.11.22})$$

The bandwidth of the cavity is labeled 3 dB bandwidth since we refer to the normalized quantity  $10 \log_{10}\left[\frac{P_{\text{diss}}(f)}{P_{\text{diss}}(f_{\text{res}})}\right]$ : the bandwidth corresponds to the frequency interval related to the  $-3 \text{ dB}$  points below the peak. In other words, dissipations and the external coupling cause the cavity to oscillate in a

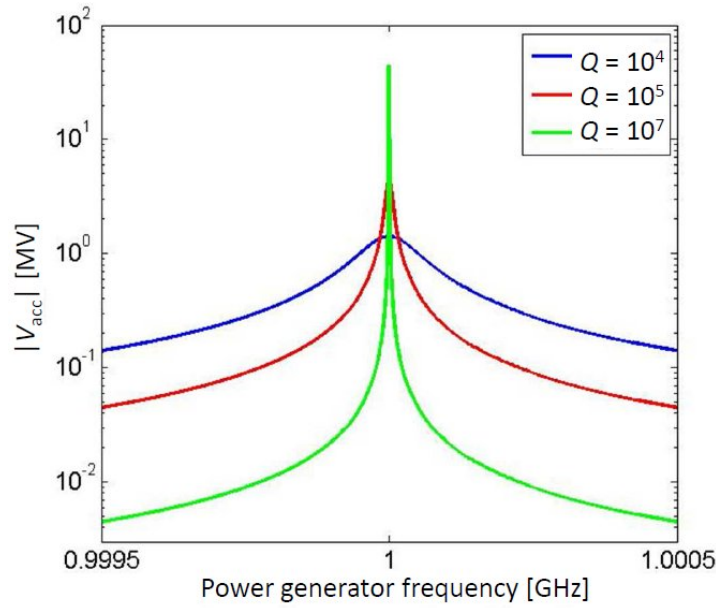


**Fig. I.11.8:** Accelerating voltage as a function of the excitation frequency for a cavity with  $\frac{R}{Q} = 100$ ,  $\beta = 1$ ,  $f_{\text{res}} = 1$  GHz, supposing that  $P_{\text{in}} = 1$  MW [10].

band of frequencies ( $\Delta f|_{3dB} = \frac{f_{\text{RF}}}{Q_L}$ ) whose width is a function of the loaded quality factor  $Q_L$ . Let us now consider a cavity powered by a source (klystron) in pulsed mode at a frequency  $f_{\text{RF}} = f_{\text{res}}$ . If we suppose that the generator is switched on at time  $t = 0$  with a peak power  $P_{\text{in}}$  we obtain the following expressions for the accelerating voltage, and dissipated and reflected powers [1]

$$\left\{ \begin{array}{l} \hat{V}_{\text{acc}}(t) = \frac{2\sqrt{\beta}}{1+\beta} \left(1 - e^{-\frac{t}{\tau}}\right) \sqrt{R P_{\text{in}}} \\ P_{\text{diss}}(t) = P_{\text{in}} \frac{4\beta}{(1+\beta)^2} \left(1 - e^{-\frac{t}{\tau}}\right)^2 \\ P_{\text{refl}}(t) = P_{\text{in}} \left[ \left(1 - e^{-\frac{t}{\tau}}\right) \frac{2\beta}{1+\beta} - 1 \right]^2 \end{array} \right. \xrightarrow{\beta=1} \left\{ \begin{array}{l} \hat{V}_{\text{acc}}(t) = \left(1 - e^{-\frac{t}{\tau}}\right) \sqrt{R P_{\text{in}}} \\ P_{\text{diss}}(t) = P_{\text{in}} \left(1 - e^{-\frac{t}{\tau}}\right)^2 \\ P_{\text{refl}}(t) = P_{\text{in}} e^{-\frac{2t}{\tau}} \end{array} \right. , \quad (\text{I.11.23})$$

where  $\tau$  is the filling time:  $\tau = \frac{2Q_L}{\omega_{\text{res}}}$ .

The behaviour for a 1 GHz NC cavity with a quality factor  $Q_0 = 3 \times 10^4$  is given in Fig. I.11.9, where the accelerating voltage is fixed and the dissipated and reflected powers are given as a function of time, assuming  $\beta = 1$ . In the plot we fixed the accelerating voltage at regime equal to  $\hat{V}_{\text{acc}} = 1$  MV and we have calculated from Eq. (I.11.19) the required input power to reach this value. In the same plot is also shown, for reference, a quality factor  $3 \times 10^5$  that is at least, four orders of magnitude lower than the Q-factor of a typical superconducting structure. The plots and the previous formulas clearly show the following important results:

1. The input power we need to reach the desired voltage is inversely proportional to the quality factor

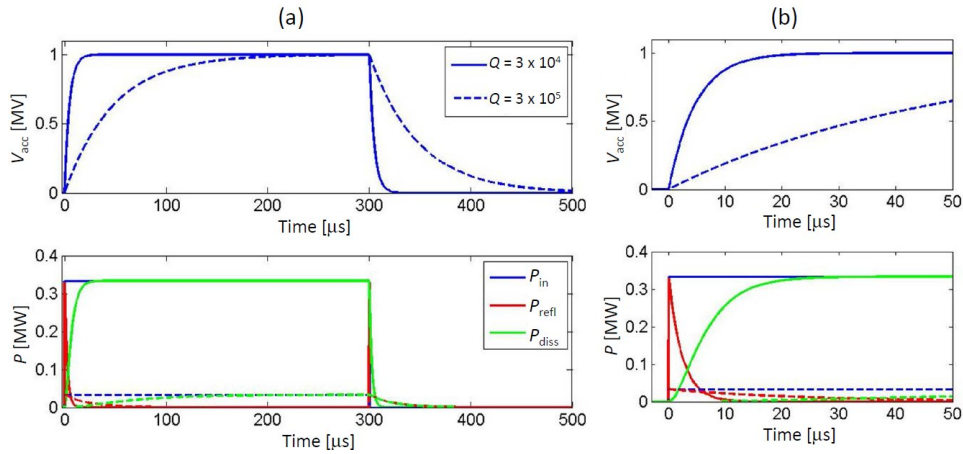


**Fig. I.11.9:** Accelerating voltage and dissipated and reflected powers as a function of time for two different values of the cavity quality factors,  $\frac{R}{Q} = 100$ ,  $\beta = 1$ ,  $f_{\text{res}} = 1$  GHz and an accelerating voltage at regime  $\hat{V}_{\text{acc}} = 1$  MV [10].

of the cavity according to

$$P_{\text{in}} = \frac{\hat{V}_{\text{acc}}^2}{\left(\frac{R}{Q}\right)} \frac{1}{Q_0} \propto \frac{1}{Q_0}, \quad (\text{I.11.24})$$

and the dissipated power into the structure follows the same scaling. This means that, as an example, to reach a 1 MV accelerating voltage with a NC cavity at 1 GHz we need an input power of the order of a few hundred kW, while for a superconducting cell it scales to a few W.

2. There is a peak of reflected power back to the generator at the beginning (and at the end) of the input pulse that requires protection for the generator itself to avoid damages. In the waveguide line, to this purpose, we use isolators (or circulators).
3. The voltage in the cavity grows with a filling time proportional to the quality factor of the cavity  $\tau = \frac{2Q_L}{\omega_{\text{res}}}$ .

Typical filling times for NC cavities are of the order of a microsecond while for a SC cavity they are hundreds of milliseconds. This is also the reason why it is difficult to represent, in the same plot, a NC cavity and an SC one, and why we have chosen a value of  $Q_0 = 3 \times 10^5$  instead of a value of  $10^9$  to  $10^{10}$ .

### I.11.6.3 Multi-cell SW cavities

In linacs, RF cavities are used in systems of multi-cavities. In a multi-cell structure, there is one input coupler that feeds a system of coupled cavities as sketched in Fig. I.11.10. The field of adjacent cells is coupled through the cell irises (and/or through properly designed coupling slots). It is quite easy to demonstrate that, for such structures the shunt impedance is approximately  $N$  times the impedance of a single cavity. With one RF source, it is possible to feed a set of cavities with a simplification of the power distribution system layout. However the fabrication of multi-cell structures is more complicated than single-cell cavities.

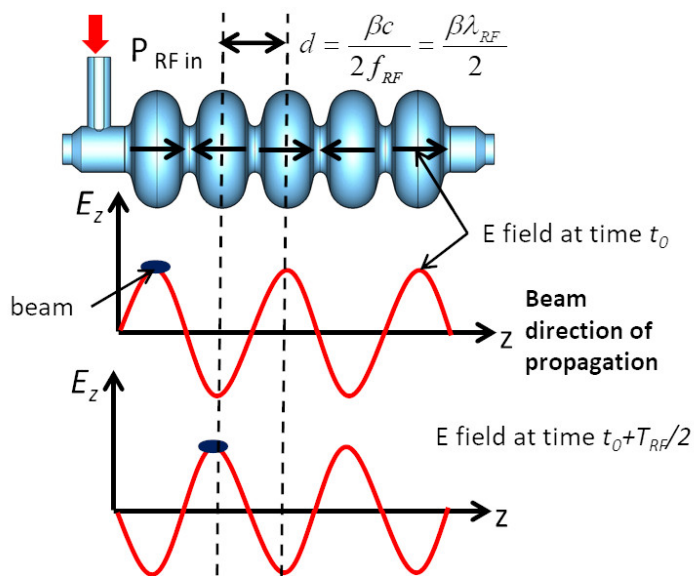


**Fig. I.11.10:** Acceleration  $a$  in multi-cell SW cavity operating in the  $\pi$ -mode: the cell length is equal to  $\beta \lambda_{RF}/2$  and the bunch in each cell is always synchronous with the electric field positive half-wave [10].

### I.11.6.3.1 $\pi$ -mode structures

An  $N$ -cell structure behaves like a system of  $N$  coupled oscillators with  $N$  coupled multi-cell resonant modes. As an example, the field configuration of a two-cell resonator is shown in Fig. I.11.11. The mode in which the two cells oscillate with the same phase is called 0 mode, while the one with  $\pi$  phase shift is called  $\pi$ -mode. It is quite easy to verify that the most efficient configuration (generally used for acceleration) is the  $\pi$ -mode, which is shown in Fig. I.11.11 for a system of five cells.

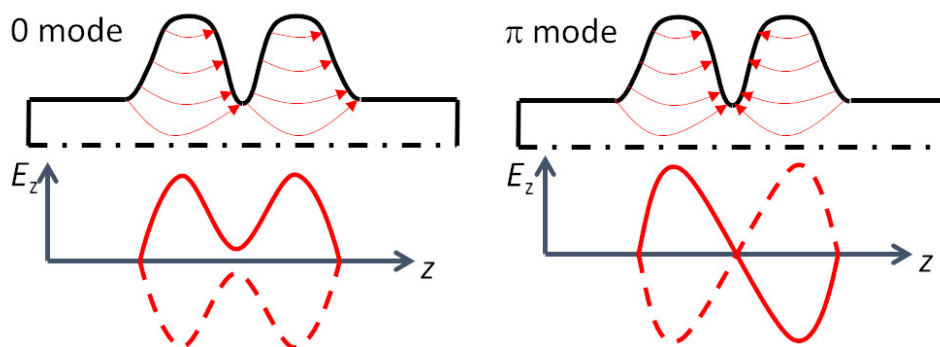


**Fig. I.11.11:** Resonant modes in a system of two coupled cavities. The mode typically used for acceleration is the  $\pi$ -mode [10].

In this system, in order to have a synchronous acceleration in each cell, the distance ( $d$ ) between the centre of two adjacent cells has to be  $d = \frac{v}{(2f_{RF})}$  where  $v$  is the particle velocity. As sketched in Fig. I.11.10 this allows to synchronize the beam passage in each cell with the accelerating field, granting a continuous acceleration process.

To maintain the synchronism, for ions and protons the cell length has to be increased and the

linac will be made of a sequence of different accelerating structures matched to the ion/proton velocity. For electrons, after the injector,  $d = \lambda_{\text{RF}}/2$  and the linac is made by a series of identical accelerating structures. Field amplitude variation from cell to cell should be also small, to maximize the acceleration efficiency. This requires a careful realization procedure, which is sometimes not sufficient to reach field flatness below a few percent, and thus requires a tuning process after fabrication. Examples of this type of system are the Linac4 (CERN) PIMS (PI Mode Structure) that operates at  $f_{\text{RF}} = 352$  MHz with  $\beta > 0.4$  [18] and, for electrons, the superconducting cavities of the European X-FEL that operate with modules of nine coupled cells at 1.3 GHz [21, 22].

### I.11.6.3.2 $\pi/2$ mode structures

It is possible to demonstrate that in a multi-cell system the different resonant modes are distributed on a curve called “dispersion curve”. As an example, the case of a 9-cell structure is shown in Fig. I.11.12.

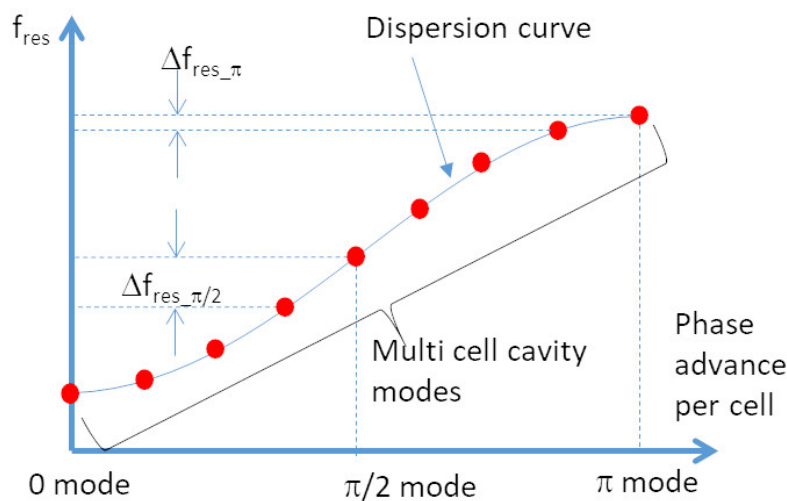


**Fig. I.11.12:** Resonant modes distributed on the “dispersion curve” for a 9-cell multi-cell structure [10].

Each mode has a bandwidth proportional to the quality factor and, over a certain number of coupled cavities, the overlap of the tails of adjacent modes can introduce problems for field equalization and structure operability. This limits the maximum number of multi-cell structures to around 10–15. Since the criticality of a working mode depends on the frequency separation between the working mode and the adjacent modes, the  $\pi/2$  mode, from this point of view, is the most “stable” one. Unfortunately, for this mode it is possible to demonstrate that the accelerating field is zero every two cells. One possible solution to use this mode is to put off-axis the empty cells (called coupling cells) like in the system schematically represented in Fig. I.11.13(a). In spite of this mechanical complication with respect to a  $\pi$ -mode system (see as example the mechanical drawing of Fig. I.11.13(b)), this allows to increase the number of cells to more than 20 without problems.

These types of structures are used both for electrons and protons. As an example, in the Spallation Neutron Source (SNS) [23] a Coupled Cavity Linac (CCL) section is used with 4 modules, each containing 12 accelerator segments. It operates at 805 MHz and accelerates the proton beam from 87 to

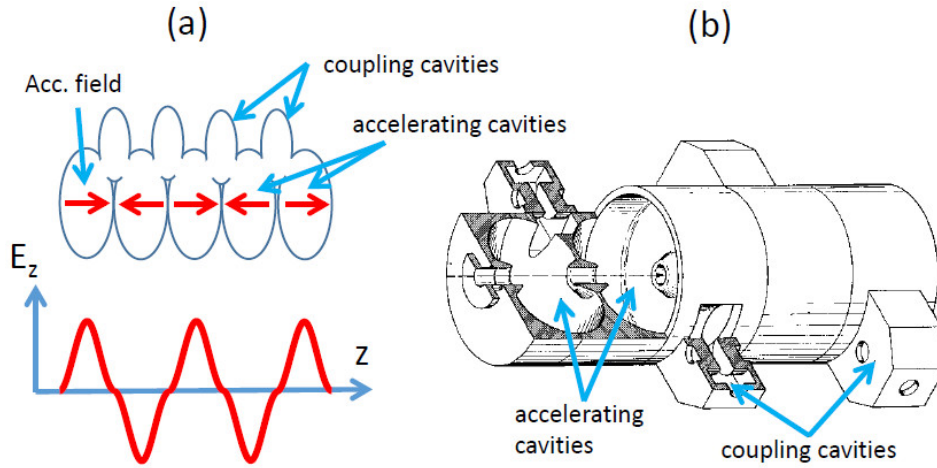


**Fig. I.11.13:** (a) Schematic drawing of a multi-cell cavity of 5 cells operating on the  $\pi/2$  mode; (b) Perspective mechanical drawing of the cavity [10].

186 MeV over a length of about 55 metres.

### I.11.7 Travelling wave structures

There is another possibility to accelerate particles: using travelling wave (TW) structures. In TW structures, an e.m. wave travels together with the beam in a special guide in which the phase velocity of the wave matches the particle velocity. In this case, the beam absorbs energy from the wave and it is continuously accelerated. Typically, these structures are used for electrons because for such particles the velocity can be assumed constant all along the structure and equal to  $c$ , while it would be difficult to modulate the phase velocity for heavy particles that change their velocity during acceleration. In the simple case of an e.m. wave propagating into a constant cross-section waveguide, the phase velocity is always larger than the speed of light and thus the e.m. wave will never be synchronous with a particle beam. As an example in a circular waveguide (Fig. I.11.14(a)) the first propagating mode with  $E_z \neq 0$  is the  $TM_{01}$  mode, whose longitudinal electric field (neglecting attenuation) can be expressed by the well known formula [24]

$$\begin{cases} E_z|_{TM_{01}} &= E_0 J_0\left(\frac{p_{01}}{a} r\right) \cos(\omega_{RF} t - k_z^* z) \\ k_z^* &= \frac{1}{c} \sqrt{\omega_{RF}^2 - \omega_{cut}^2} \end{cases}, \quad (\text{I.11.25})$$

where  $a$  is the radius of the waveguide,  $k_z^*$  is the propagation constant,  $\omega_{cut}$  is the cut-off angular frequency of the waveguide equal to  $\omega_{cut} = \frac{c p_{01}}{a}$ .

The corresponding phase velocity is given by

$$v_{ph} = \frac{\omega_{RF}}{k_z^*} = \frac{c}{\sqrt{1 - \frac{\omega_{cut}^2}{\omega_{RF}^2}}}, \quad (\text{I.11.26})$$

which is always larger than  $c$ . The behaviour of the propagation constant as a function of frequency is the well-known dispersion curve plotted in Fig. I.11.14(a). It is worth reminding that the phase velocity

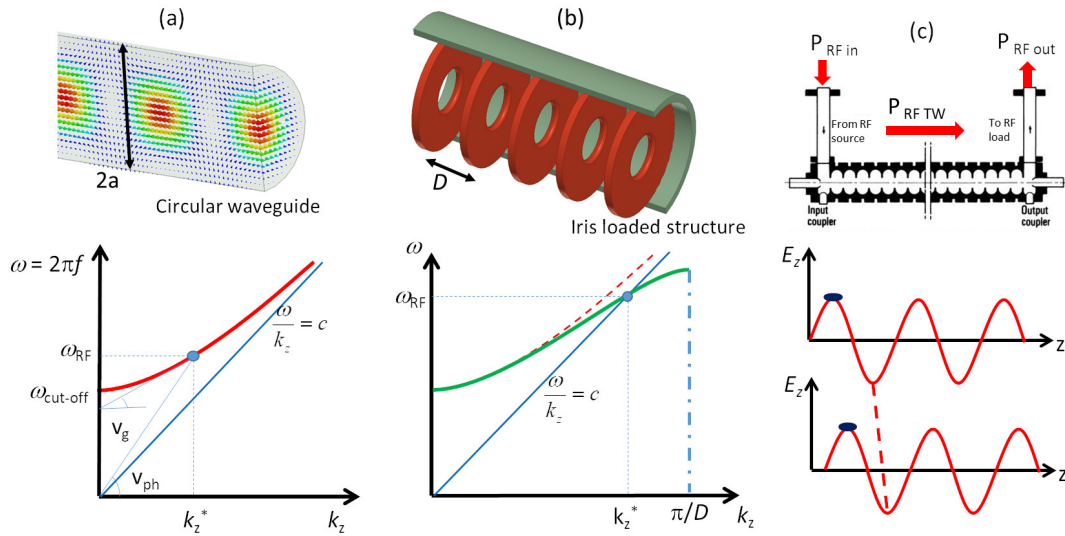


**Fig. I.11.14:** TW structures: (a) Circular waveguide example (top) and its dispersion curve (bottom); (b) Iris loaded waveguide model (top) and its typical dispersion curve (bottom); (c) TW structure with input and output couplers: the e.m. field travels together with the bunch, continuously transferring its energy to the particles [10].

is not the velocity of the energy propagation in the structure, which, instead, is the group velocity ( $v_g$ )

$$v_g = \left. \frac{d\omega}{dk_z} \right|_{\omega=\omega_{\text{RF}}} = c \sqrt{1 - \frac{\omega_{\text{cut}}^2}{\omega_{\text{RF}}^2}}, \quad (\text{I.11.27})$$

and it is always smaller than  $c$ .

In order to slow down the wave phase velocity, the structure through which the wave is travelling, is periodically loaded with irises. A sketch of an iris-loaded structure is given in Fig. I.11.14 (b). A structure can be designed to have the phase velocity equal to the speed of the particles allowing a net acceleration over large distances. The propagating field, in this case, is that of a special wave travelling within a spatial periodic profile (TM<sub>01</sub>-like mode) and, according to Floquet's theorem [1, 2, 24] can be expressed as

$$E_z|_{\text{TM}_{01}\text{-like}} = E_P(r, z) \cos(\omega_{\text{RF}} t - k_z^* z) e^{-\alpha z}, \quad (\text{I.11.28})$$

with  $E_P(r, z)$  a periodic function with period  $D$ . In Eq. (I.11.28) the propagating constant does not have an analytical expression as in the case of a constant cross-section waveguide and the dispersion curve for this type of structures is given in Fig. I.11.11(b) and shows that, at a given frequency, the phase velocity can be equal to (or even slower than)  $c$ . In Eq. (I.11.28),  $\alpha$  [m<sup>-1</sup>] is the attenuation constant of the accelerating field due to RF losses in the metal walls. Typical values of  $\alpha$  are in the range 0.2–0.3 [m<sup>-1</sup>].

In a TW structure, the RF power enters into the cavity through an input coupler and flows through the cavity in the same direction as the beam. An output coupler, at the end of the structure, connected to a matched load, absorbs the residual power not transferred to the beam or dissipated in the cavity wall,

avoiding reflections: this is sketched in Fig. I.11.11(c). If there is no beam, the input power dissipates partly in the cavity walls and the remainder is then dissipated into the power load. In the presence of a beam current a fraction of this power is, indeed, transferred to the beam itself. TW structures allow acceleration over large distances (few metres, hundreds of cells) with just an input coupler and a relatively simple geometry.

For example, the SLAC electron linac [25] is composed by more than one hundred 3 m long structures operating at 2.856 GHz while the SwissFEL linac has 96 structures, 2 m long operating at 5.712 GHz [26–28]. Similarly to what has been done for SW cavities, it is possible to define some figures of merit for TW structures.

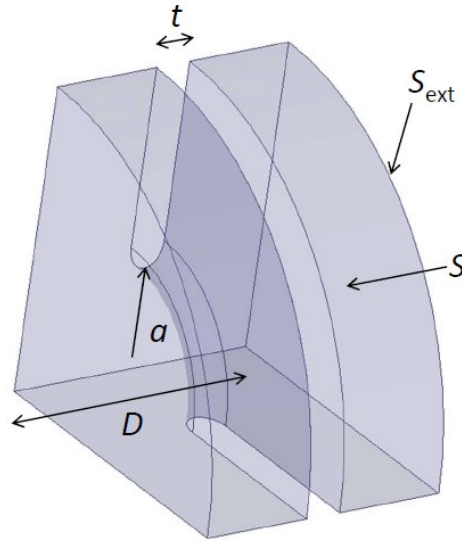


**Fig. I.11.15:** TW structures: sketch of a quarter of a single-cell of a TW structure.

Referring to the single cell sketched in Fig. I.11.15, we consider the following quantities [29]

$$\begin{aligned}
 \hat{V}_{\text{acc}} &= \left| \int_0^D E_z e^{j\omega_{\text{RF}} \frac{z}{c}} dz \right| && \text{single cell accelerating voltage [V]} \\
 \hat{E}_{\text{acc}} &= \frac{\hat{V}_{\text{acc}}}{D} && \text{average accelerating field in the cell [V/m]} \\
 P_F &= \int_S \frac{1}{2} \text{Re} \left( \vec{E} \times \vec{H}^* \right) \cdot \hat{z} dS && \text{power flow [W]} \\
 P_{\text{diss}} &= \frac{1}{2} R_s \int_{\text{cavity wall}} |H_{\text{tan}}|^2 dS && \text{average dissipated power in the cell [W]} \\
 p_{\text{diss}} &= \frac{P_{\text{diss}}}{D} && \text{average dissipated power per unit length [W/m]} \\
 W &= \int_{\text{cavity volume}} \left( \frac{1}{4} \epsilon |\vec{E}|^2 + \frac{1}{4} \mu |\vec{H}|^2 \right) dV && \text{stored energy in the cell [J]} \\
 w &= \frac{W}{D} && \text{average stored energy per unit length [J/m]} \quad ,
 \end{aligned} \tag{I.11.29}$$

where  $\left( \frac{1}{4} \epsilon |\vec{E}|^2 + \frac{1}{4} \mu |\vec{H}|^2 \right)$  is the energy density in the cavity.

The shunt impedance per unit length  $r$  (similarly to Eq. (I.11.16) for SW cavities) is defined as

$$r = \frac{\hat{E}_{\text{acc}}^2}{p_{\text{diss}}} \left[ \frac{\Omega}{m} \right] . \quad (\text{I.11.30})$$

The higher the value of  $r$ , the higher the available accelerating field for a given RF power. Typical values for a 3 GHz structure are  $\sim 60 - 70 \text{ M}\Omega/\text{m}$ . The attenuation constant  $\alpha$ , is defined as

$$\alpha = \frac{p_{\text{diss}}}{2 P_F} \left[ \frac{\Omega}{m} \right] . \quad (\text{I.11.31})$$

In a purely periodic structure, made by a sequence of identical cells (also called a “constant impedance structure”), the RF power flux and the intensity of the accelerating field decay exponentially along the structure. The process of power filling is represented in Fig. I.11.16.

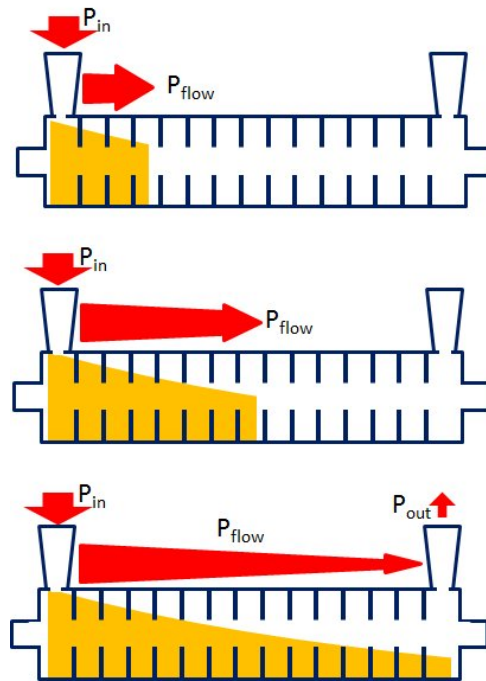


**Fig. I.11.16:** TW structures: illustration of the power filling for a TW structure.

When the RF generator is switched on, the power starts flowing into the structure with a velocity equal to the group velocity, which is typically a small fraction of the velocity of light (a few percent). The time necessary to propagate the RF wavefront from the input coupler to the end of a section of length  $L$ , referred to as the filling time, is given by

$$\tau_F = \frac{L}{v_g} \quad [\text{s}] . \quad (\text{I.11.32})$$

Typical values of the group velocity  $v_g$  are 1–2% of the speed of light and, as a consequence, the filling times are of the order of few hundreds of ns up to 1  $\mu\text{s}$ . After one filling time the structure is completely filled of e.m. energy and the beam can be injected and efficiently accelerated. It is quite easy to

demonstrate (see exercise 5) that the group velocity can be calculated by

$$v_g = \frac{P_F}{w} \left[ \frac{\text{m}}{\text{s}} \right] . \quad (\text{I.11.33})$$

Increasing the group velocity allows a reduction of the duration of the RF pulse powering the structure. Since  $w \propto E^2$ , however, a low group velocity is preferable to increase the effective accelerating field for a given power flowing in the structure. It is possible to demonstrate that the group velocity scales as  $a^3$  where  $a$  is the iris's aperture [1]. It is also possible to define a quality factor for TW structures

$$Q = \omega_{\text{RF}} \frac{w}{p_{\text{diss}}} , \quad (\text{I.11.34})$$

which can with Eqs. (I.11.31) and (I.11.33) be expressed in term of the attenuation constant  $\alpha$

$$Q = \frac{\omega_{\text{RF}}}{2v_g\alpha} . \quad (\text{I.11.35})$$

Each structure is also identified by a field phase advance per cell given by  $\Delta\phi = k_z^*$ . For several reasons discussed in [25], one of the most common modes used for acceleration is  $2\pi/3$ . It can be demonstrated that (see exercise 5) the average accelerating field in a simple TW structure, can be expressed as

$$\hat{E}_{\text{acc}} = \sqrt{2\alpha r P_{\text{in}}} e^{-\alpha z} . \quad (\text{I.11.36})$$

$P_{\text{in}}$  is the input power into the structure, while the power flowing into the structure scales as

$$P_F(z) = P_{\text{in}} e^{-2\alpha z} . \quad (\text{I.11.37})$$

The total accelerating voltage is then given by

$$\hat{V}_{\text{acc}} = \hat{E}_{\text{in}} \frac{1 - e^{-\alpha L}}{\alpha} . \quad (\text{I.11.38})$$

As an example, we consider a 2 m long C-band ( $f_{\text{RF}} = 5.712$  GHz) accelerating section made of copper. Using an iris aperture of  $2a = 14$  mm, we obtain for the  $2\pi/3$  mode typical values of the above mentioned parameters:  $r = 82$  [M $\Omega$ /m],  $\alpha = 0.36$  [m $^{-1}$ ],  $v_g/c = 1.7\%$ . This gives a filling time of  $\tau_F = 150$  ns, which is much lower than typical values obtainable with SW structures working at the same frequency. Figure I.11.17(a) shows the power flow along the structure, and the corresponding accelerating field, assuming a pulsed input power of 50 MW. The power dissipated into the structure and the total accelerating voltage integrated by a particle entering into the section at different times are shown in Fig. I.11.17(b). In the figure, it is possible to observe that after one filling time the structure is full of energy, and the integrated voltage seen by a particle does not change. At the other end of the structure, the remaining power has to be dissipated into an external load to avoid reflections. These, in fact, can be reflected back to the RF power unit (causing possible damages), increase the peak fields locally (causing possible discharges) or can produce undesirable perturbations to the beam dynamics. Typically, TW structures have very short filling time values ( $< 1$   $\mu$ s) and allow operation in pulsed mode at low repetition rate (10 Hz to 100 Hz) with high peak power (tens of MW) and relatively high

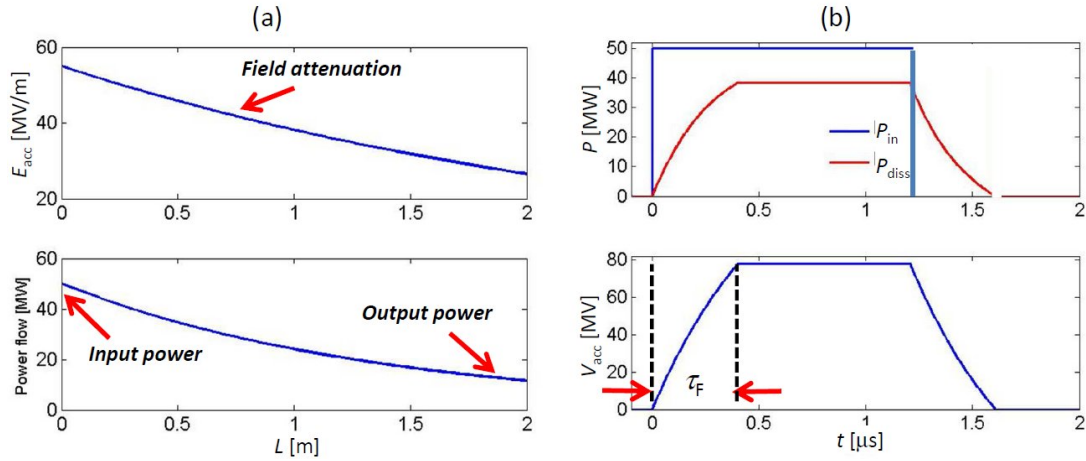


**Fig. I.11.17:** TW structures: (a) Accelerating field and power flow; (b) input power, cavity dissipated power and accelerating voltage, for a C-band constant impedance structure working on the  $2\pi/3$  mode.

accelerating field (up to 50 MV/m). In conclusion, note the following important remarks:

1. Due to the power dissipation and the consequent reduction of the accelerating field, increasing the TW cavity length at the end makes the acceleration process very inefficient. Typically in the S-band (3 GHz) the cavity length is limited to 3 m, in the C-band (6 GHz) to 2 m.
2. There is no benefit in selecting SC materials for TW structure fabrication. This is a direct consequence of the TW working principle, where the accelerating field build-up is not affected or limited by ohmic losses. The obtainable gain using SC materials is thus not relevant. It would be, theoretically, only using a very long TW structure, but this would imply very long RF pulses at high peak voltage (not feasible) together with a dramatic complication of the realization process.
3. Since the structure is basically a waveguide with irises, at the input port there are no significant power reflections towards the generator, and thus it is possible to connect the power unit directly to the section without circulators/isolators to protect the source.

In Appendix I it is also shown how the SW field of a multi-cell structure can be written as the sum of two counter propagating travelling waves.

#### ***1.11.7.0.1 Travelling wave constant gradient structures***

An example of a constant impedance TW structure has been presented in the previous section. Irises of equal dimensions cause the accelerating field to decay exponentially along the section. It is possible to demonstrate that, in order to keep the accelerating field constant in the whole structure, the iris aperture has to be properly shrunk along the structure [1, 25, 29]. This can be intuitively understood looking at the Eq. (I.11.33) that we rewrite here as

$$\frac{P_F}{v_g} = w \propto E_{acc}^2 \quad .$$

The power flow  $P_F$  attenuates along the structure according to Eq. (I.11.37) and, therefore, in order to have a constant accelerating field  $E_{acc}$ ,  $v_g$  has also to decrease along the structure. In this way, the field attenuation is compensated for by an increase of the stored energy per unit length, due to the lower group velocity. For instance, Figure I.11.18 shows the iris dimensions and the section parameters for a 100-cell C-band constant gradient and constant impedance structure as a function of the cell number. In both cases the average accelerating field is the same and equal to 40 MV/m for 50 MW input power. Because of the different iris dimensions, the group velocity and shunt impedance also change along the structure.

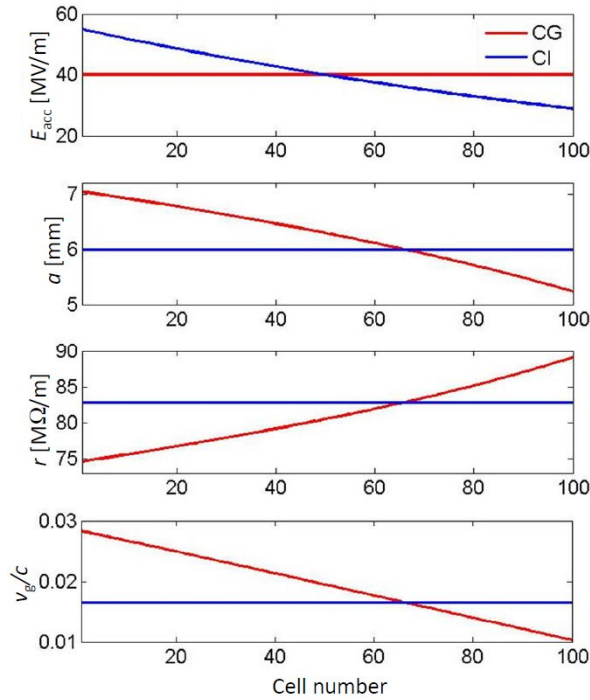


**Fig. I.11.18:** Iris dimensions and structure parameters for 100-cell C-band constant gradient (red line) and constant impedance (blue line) structures [10].

In general, constant gradient structures are more efficient than constant impedance structures, because of the more uniform distribution of RF power in the longitudinal direction, but they require a more complicated mechanical realization due to the irises' profile modulation. The parameters of the TW accelerating structures of the SLAC linac [25] (used for the LCLS FEL), the PSI SwissFEL [26–28] and Spring 8 XFEL linac [30, 31] can be found as examples in [20].

### I.11.8 Linac technology

In the previous sections the main characteristics of the accelerating structures with their main figures of merit, properties and geometries have been illustrated. We will now go into the details of linac technology, starting with the material generally used for the structure's realization. As already pointed out the most common alternatives are oxygen-free high conductivity (OFHC) copper for NC cavities, and niobium for the SC ones.

### I.11.8.1 Oxygen-free high conductivity copper OFHC

OFHC copper is the most common material used for NC structures for several reasons:

1. It has a very good electrical (and thermal) conductivity;
2. It has a low secondary emission yield (SEY) that allows to reduce multiple impact electron amplification (multipacting) phenomena [32] during structures power up, conditioning and operation;
3. It shows good performance at a high accelerating gradient;
4. It is easy to machine, and a very good roughness (up to the level of a few nm) can be achieved;
5. It can be brazed or welded.

The microwave surface resistance of the copper (as for all metals) is expressed by

$$R_s = \sqrt{\frac{\pi f_{\text{RF}} \mu_0}{\sigma}} = \frac{1}{\sigma \delta} \quad , \quad (\text{I.11.39})$$

where  $\sigma$  is the conductivity ( $\sim 5.8 \times 10^7$  S/m for Cu at 20°C),  $\mu_0 = 4\pi 10^{-7}$  H/m and  $\delta$  is the skin depth, which represents the penetration of the e.m. field and surface currents inside the metal, (see Fig. I.11.19 (a)), given by

$$\delta = \frac{1}{\sqrt{\pi f_{\text{RF}} \mu_0 \sigma}} \quad . \quad (\text{I.11.40})$$

The behaviour of the surface resistance and skin depth as a function of frequency is shown in Fig. I.11.19(b). The conductivity increases when the temperature is reduced. In the DC regime it can

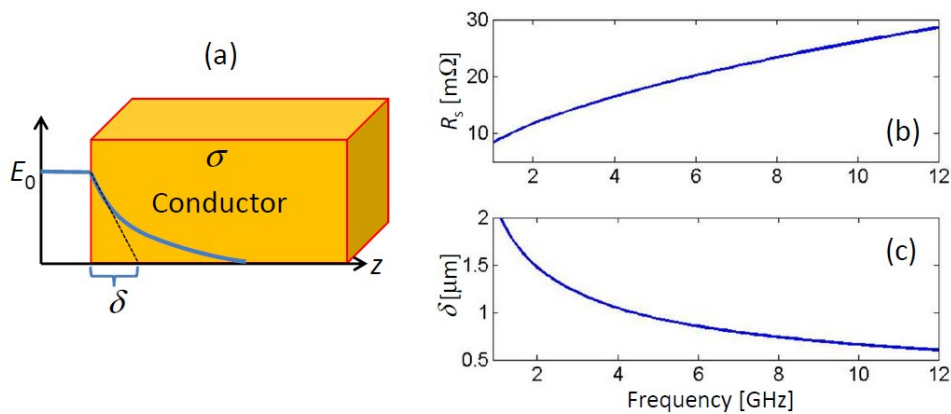


**Fig. I.11.19:** (a) Sketch of the penetration of RF EM fields and surface currents inside a metal; behaviour of (b) copper surface resistance and (c) skin depth as a function of frequency [10].

be more than a factor of 100 higher (depending on the copper purity) at cryogenic temperatures than at room temperature. At cryogenic temperatures ( $< 40$  K) and in the RF regime, however, a mechanism called the *anomalous skin effect* [33] takes place reducing the gain in conductivity to a factor of about 20 (depending on the working frequency and copper purity). This will also translate into a reduction of the gain in the quality factor: this makes the use of copper at cryogenic temperatures neither practical nor convenient.

### I.11.8.2 Niobium

Superconductivity was discovered in 1911. For a SC material below its critical temperature  $T_c$ , in the DC regime, the resistance is zero. In the RF regime, however, the surface resistance is always larger than zero (even if orders of magnitude lower than NC materials), because not all the electrons are in the superconducting state. The residual ones are not completely shielded by the superconducting currents and thus experience a residual electric field, dissipating power. At frequencies below 10 GHz (and temperatures below  $T_c/2$ ), the experimental data available for several materials are well described by the empirical relation [34–40]

$$R_s = \underbrace{A \frac{\omega_{\text{RF}}^2}{T}}_{R_{\text{BCS}}} e^{-\alpha \frac{T_c}{T}} + R_{\text{res}} \quad . \quad (\text{I.11.41})$$

The first term, the resistance  $R_{\text{BCS}}$ , is well explained by a theoretical model of the superconductor. In this term the coefficients  $A$  and  $\alpha$  depend on the material. The second term is a residual term due to impurities in the material. The SC state can be destroyed by an external magnetic field larger than a critical field  $H_c$  that depends on the material used. In practice, this effect fixes the maximum theoretical field that a SC cavity can sustain. The most common material for the fabrication of SC cavities is niobium for several reasons [38–40] since Nb:

1. Has a relatively high transition temperature ( $T_c = 9.25$  K);
2. Has a relatively high critical magnetic field,  $H_c = 170$  mT to 180 mT;
3. Is chemically inert;
4. Can be machined and deep drawn;
5. Is available either as bulk or sheet in any size, fabricated by forging and rolling;
6. With large grain size (often favoured) can be obtained by e-beam melting;
7. Can also be used as a coating (e.g. by sputtering) on NC materials like Cu;
8. Has good thermal stability and is of relatively low cost.

The  $R_{\text{BCS}}$  resistance for Nb is given by:

$$R_{\text{BCS}} = 2 \times 10^{-4} \frac{\left(\frac{f_{\text{RF}}[\text{MHz}]}{1500}\right)^2}{T} e^{-\frac{17.67}{T}} \quad [\Omega] \quad (\text{I.11.42})$$

and the residual resistance can vary between 5 nΩ and 20 nΩ. The behaviour of niobium resistance as a function of temperature at 700 MHz is shown in Fig. I.11.20.

### I.11.9 Beam structure and RF structure

RF structures are fed, in general, by pulses with a certain repetition rate and duty cycle (DC), which is defined as the ratio between the pulse width  $T_{\text{rf\_pulse}}$  and the period  $T_{\text{rep}}$  ( $\text{DC} = T_{\text{rf\_pulse}}/T_{\text{rep}}$ ). Each pulse may include from thousands up to several million RF periods as schematically represented in

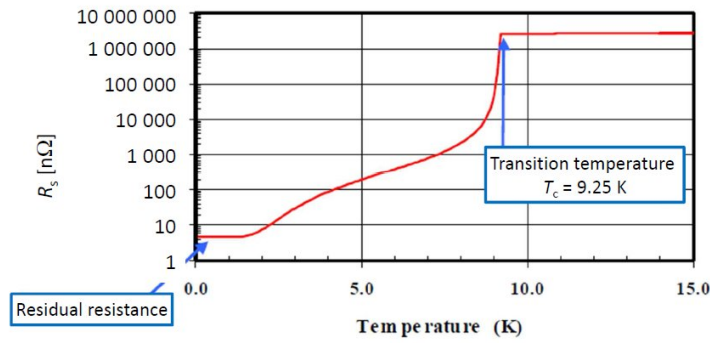


**Fig. I.11.20:** Surface resistance of Nb at 700 MHz (taken from Ref. [36]).

Fig. I.11.21(a). The “beam structure” in a linac is correlated to the “RF structure” since a fraction of the RF pulse is used for beam acceleration (as represented in Fig. I.11.21(b)).

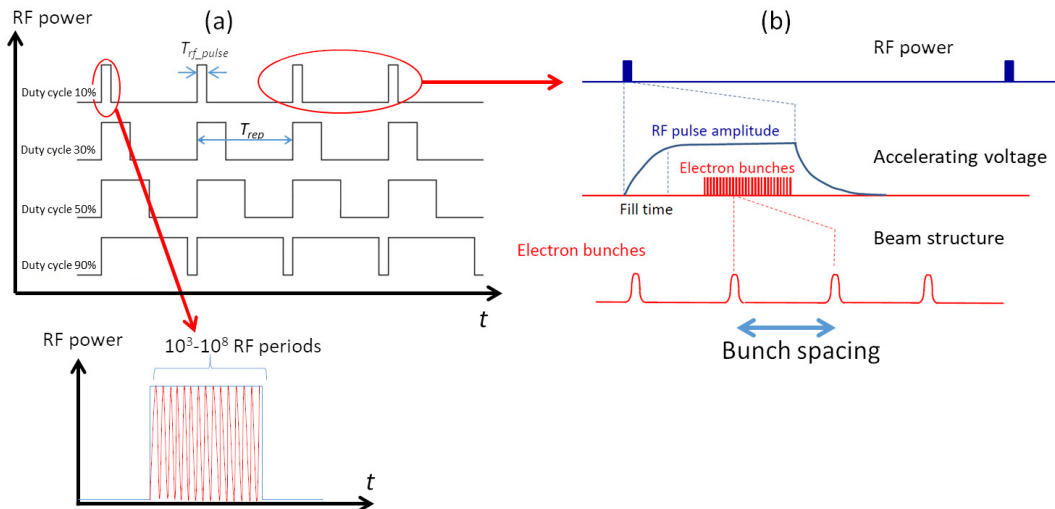


**Fig. I.11.21:** (a) Sketch of the input RF power into accelerating structures and (b) related beam structure [10].

SC structures allow operation at very high DC ( $> 1\%$ ) up to a continuous wave (CW) operation (DC = 100 %), because of the extremely low dissipated power, with relatively high accelerating field ( $> 20$  MV/m). This means that a continuous (bunched) beam can be accelerated. NC structures can operate in pulsed mode at lower DC ( $< 0.1\%$ ), because of the higher dissipated power with, in principle, larger peak accelerating field ( $> 30$  MV/m). In low DC linacs, depending on the application, from one up to few-hundred bunches can be, in general, accelerated.

Typically, TW structures have very short filling time values ( $< 1 \mu\text{s}$ ) and allow operation in pulsed mode at low repetition rate (from 10 Hz to 100 Hz) with high-peak power (tens of MW) and relatively high accelerating field (up to 50 MV/m). Typical DC are very low ( $10^{-4}$  to  $10^{-5}$ ). For instance, assuming the previously mentioned TW structure being fed by 400 ns RF pulses of 50 MW ( $P_{\text{in}}$ ) at 100 Hz, the resulting DC is  $4 \times 10^{-5}$  with a total average power from the RF generator of 2 kW ( $P_{\text{in}} \times \text{DC}$ ). The

use of short RF pulses, however, gives the possibility of accelerating just a few bunches per RF pulse.

### I.11.10 Longitudinal beam dynamics of accelerated particles

In this second part of the paper the basic principles of the longitudinal and transverse beam dynamics will be illustrated. A complete dissertation can be found in Refs. [1,2,41].

#### I.11.10.1 Synchronous phase

Let us consider a SW linac structure made by accelerating gaps (like a DTL) or cavities as shown in Fig. I.11.22(a). In each gap the accelerating field oscillates in time and the accelerating voltage ( $V_{acc}$ ), plotted in Fig. I.11.22(b) can be expressed as

$$V_{acc} = \hat{V}_{acc} \cos(\omega_{RF}t) \quad . \quad (I.11.43)$$

We can assume that a “perfect” synchronism condition is fulfilled for an ideal particle that crosses each gap with a phase  $\phi_s$  with respect to the accelerating voltage. By definition this phase is called *synchronous phase* and the particle, the *synchronous particle*. Then when the synchronous particle enters in each gap with a phase  $\phi_s$  ( $\phi_s = \omega_{RF}t_s$ ) with respect to the RF voltage, it has an energy gain (and a consequent change in velocity) that allows it to enter in the subsequent gap with the same phase  $\phi_s$  with respect to the accelerating voltage and so on. For this particle the energy gain in each gap is given simply by

$$\Delta E = q \underbrace{\hat{V}_{acc} \cos(\phi_s)}_{V_{acc-s}} = qV_{acc-s} \quad . \quad (I.11.44)$$

Looking at the plot of Figure I.11.22 one may easily understand that both  $\phi_s$  and  $-\phi_s$  are synchronous phases.

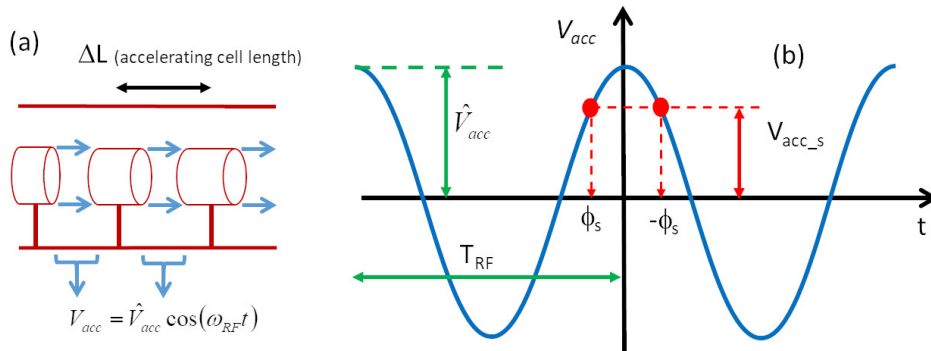


**Fig. I.11.22:** (a) Sketch of accelerating gaps; (b) accelerating voltage in each gap [10].

Let us consider the first synchronous phase  $\phi_s$  (on the positive slope of the RF voltage). If we consider a *non-synchronous* particle “near” the synchronous one, that arrives later in the cavity gap ( $t_1 > t_s$ ), this particle will experience a higher voltage (i.e. it will gain a slightly larger amount of energy) and thus will have a higher velocity than the synchronous one. Its time of flight to next gap will be shorter, partially compensating its initial delay with respect to the synchronous particle. Similarly, if we

consider a particle that enters the gap before the synchronous one ( $t_1 < t_s$ ), it will experience a smaller accelerating voltage, gaining a smaller amount of energy and its time of flight to next gap will increase, compensating the initial advantage with respect to the synchronous particle. On the contrary, if we consider the synchronous particle at phase  $-\phi_s$  and other particles “near” to this that arrive later or before in the gap, they will receive an energy gain that will increase further their distance with respect to the synchronous one. In conclusion, the synchronous phase on the positive slope of the RF voltage provides a longitudinal focusing of the beam allowing to have a stable beam acceleration. This mechanism is called *phase stability principle*. On the contrary, the synchronous phase on the negative slope of the RF voltage is an unstable position. Since it relies on particle velocity variations, longitudinal focusing does not work for fully relativistic beams (electrons). In this case acceleration *on crest* is more convenient.

### I.11.10.2 Energy-phase equations

The previous intuitive approach can find a more rigorous mathematical formalism. To this purpose, the following variables,  $\varphi$  and  $w$ , are used to describe a generic particle longitudinal position with respect to the synchronous one. They are defined as follows

$$\begin{cases} \varphi &= \phi - \phi_s = \omega_{\text{RF}}(t - t_s) \\ w &= W - W_s \end{cases}, \quad (\text{I.11.45})$$

where  $t(\phi)$  is the arrival time (phase) of a generic particle at a certain gap and  $W$  is the kinetic energy of the same particle at a certain position along the linac.  $t_s$ ,  $\phi_s$  and  $W_s$  are the quantities referred to the synchronous particle. The energy gain per *accelerating cell* (considering as “accelerating cell” one gap and two half drift tubes in case of a DTL) for the synchronous and a generic particle are respectively

$$\begin{cases} \Delta W_s = q \hat{V}_{\text{acc}} \cos \phi_s \\ \Delta W = q \hat{V}_{\text{acc}} \cos \phi = q \hat{V}_{\text{acc}} \cos(\phi_s + \varphi) \end{cases}. \quad (\text{I.11.46})$$

The delta energy gain is then given by

$$\Delta w = \Delta W - \Delta W_s = q \hat{V}_{\text{acc}} [\cos(\phi_s + \varphi) - \cos \phi_s]. \quad (\text{I.11.47})$$

Dividing by the accelerating cell length  $\Delta L$  and assuming that  $\hat{E}_{\text{acc}} = \hat{V}_{\text{acc}}/\Delta L$  is the average accelerating field over the cell (i.e. average accelerating gradient) we obtain

$$\frac{\Delta w}{\Delta L} = q \hat{E}_{\text{acc}} [\cos(\phi_s + \varphi) - \cos \phi_s] \Rightarrow \frac{dw}{dz} = q \hat{E}_{\text{acc}} [\cos(\phi_s + \varphi) - \cos \phi_s], \quad (\text{I.11.48})$$

where we have approximated  $\frac{\Delta w}{\Delta L} \approx \frac{dw}{dz}$ .

On the other hand, the phase variations per cell of a synchronous particle and of a generic particle are respectively

$$\begin{cases} \Delta \phi_s = \omega_{\text{RF}} \Delta t_s \\ \Delta \phi = \omega_{\text{RF}} \Delta t \end{cases}, \quad (\text{I.11.49})$$

where  $\Delta t$  is basically the time of flight between two accelerating cells. Considering the variation of  $\varphi$  between two accelerating gaps,  $\Delta\varphi = \omega_{\text{RF}}(\Delta t - \Delta t_s)$ , and dividing by  $\Delta L$  we have that

$$\frac{\Delta\varphi}{\Delta L} = \omega_{\text{RF}} \left( \frac{\Delta t}{\Delta L} - \frac{\Delta t_s}{\Delta L} \right) = \omega_{\text{RF}} \left( \frac{1}{v} - \frac{1}{v_s} \right) \quad (\text{I.11.50})$$

and we finally obtain<sup>1</sup>

$$\frac{\Delta\varphi}{\Delta L} \simeq \frac{d\varphi}{dz} = -\frac{\omega_{\text{RF}}}{c} \frac{w}{E_0 \beta_s^3 \gamma_s^3} \quad (\text{I.11.51})$$

Finally the system of coupled (non-linear) differential equations represented by Eqs. (I.11.48) and (I.11.50) describes the motion of a non-synchronous particle in the longitudinal plane with respect to the synchronous one

$$\begin{cases} \frac{dw}{dz} = q \hat{E}_{\text{acc}} [\cos(\phi_s + \varphi) - \cos \phi_s] \\ \frac{d\varphi}{dz} = -\frac{\omega_{\text{RF}}}{c} \frac{w}{E_0 \beta_s^3 \gamma_s^3} \end{cases} \quad (\text{I.11.52})$$

### I.11.10.3 Small-amplitude energy-phase oscillations

By calculating the derivative of the second equation of Eq. (I.11.52) with respect to  $z$  and substituting in the first equation we obtain

$$\begin{aligned} \frac{d\varphi}{dz} &= -\frac{\omega_{\text{RF}}}{c} \frac{w}{E_0 \beta_s^3 \gamma_s^3} \rightarrow c E_0 \beta_s^3 \gamma_s^3 \frac{d\varphi}{dz} = -\omega_{\text{RF}} w \\ c E_0 \beta_s^3 \gamma_s^3 \frac{d^2\varphi}{dz^2} + c E_0 \frac{d(\beta_s^3 \gamma_s^3)}{dz} \frac{d\varphi}{dz} &= -\omega_{\text{RF}} \frac{dw}{dz} \\ c E_0 \beta_s^3 \gamma_s^3 \frac{d^2\varphi}{dz^2} + c E_0 \frac{d(\beta_s^3 \gamma_s^3)}{dz} \frac{d\varphi}{dz} &= -\omega_{\text{RF}} q \hat{E}_{\text{acc}} [\cos(\phi_s + \varphi) - \cos \phi_s] \end{aligned} \quad (\text{I.11.53})$$

Assuming an adiabatic acceleration process (i.e.  $\frac{d(\beta_s^3 \gamma_s^3)}{dz} \ll 1$ ) after substitution in the second member of Eq. (I.11.53) of the first equation of Eq. (I.11.52), we obtain

$$c E_0 \beta_s^3 \gamma_s^3 \frac{d^2\varphi}{dz^2} = -\omega_{\text{RF}} q \hat{E}_{\text{acc}} [\cos(\phi_s + \varphi) - \cos \phi_s] \quad (\text{I.11.54})$$

Assuming small-amplitude oscillations around the synchronous particle, this allows to approxi-

<sup>1</sup>To obtain this result consider

$$\omega_{\text{RF}} \left( \frac{1}{v} - \frac{1}{v_s} \right) = \omega_{\text{RF}} \left( \frac{v_s - v}{v v_s} \right)$$

approximate

$$\begin{cases} v - v_s &= \Delta v \\ v v_s &\simeq v_s^2 \\ -\frac{\omega_{\text{RF}}}{v_s} \Delta v &= -\frac{\omega_{\text{RF}}}{c} \frac{\Delta\beta}{\beta_s^2} \end{cases}$$

and remember that

$$\begin{cases} \beta &= \sqrt{1 - \frac{1}{\gamma^2}} \\ \beta d\beta &= \frac{d\gamma}{\gamma^3} \\ -\frac{\omega_{\text{RF}}}{c} \frac{\Delta\beta}{\beta_s^2} &\simeq \frac{\omega_{\text{RF}}}{c} \frac{\Delta\gamma}{\beta_s^3 \gamma_s^3} = -\frac{\omega_{\text{RF}}}{c} \frac{\widehat{\Delta E}}{E_0 \beta_s^3 \gamma_s^3} \end{cases}$$

mate  $\cos(\phi_s + \varphi) - \cos \phi_s \simeq -\varphi \sin \phi_s$  and substituting this equation in Eq. (I.11.54) we finally obtain

$$\frac{d^2 \varphi}{dz^2} + q \frac{\omega_{\text{RF}} \hat{E}_{\text{acc}} \sin(-\phi_s)}{c E_0 \beta_s^3 \gamma_s^3} \varphi = 0 \quad , \quad (\text{I.11.55})$$

with

$$\Omega_s^2 = q \frac{\omega_{\text{RF}} \hat{E}_{\text{acc}} \sin(-\phi_s)}{c E_0 \beta_s^3 \gamma_s^3} \quad . \quad (\text{I.11.56})$$

We recognize the equation of an harmonic oscillator with angular spatial frequency  $\Omega_s$ . The conditions to have stable longitudinal oscillations and acceleration at the same time are then

$$\left. \begin{array}{l} \Omega_s^2 > 0 \Rightarrow \sin(-\phi_s) > 0 \\ V_{\text{acc}} > 0 \Rightarrow \cos(\phi_s) > 0 \end{array} \right\} \Rightarrow -\frac{\pi}{2} < \phi_s < 0 \quad . \quad (\text{I.11.57})$$

Equations (I.11.55) to (I.11.57) summarize what we have intuitively described with the *phase stability principle*: if we accelerate on the rising part of the positive RF wave we have a longitudinal force keeping the beam *focused* around the synchronous phase and oscillating during acceleration with spatial angular frequency  $\Omega_s$ .  $\Omega_s$  represents also the longitudinal phase advance per unit length. The angular frequency can be simply obtained substituting in Eq. (I.11.33)  $z$  with  $\beta_s c t$  (and then  $dz = \beta_s c dt$ ) and it is related to the angular spatial frequency by:  $\Omega_T = \Omega_s \beta_s c$ . The longitudinal oscillation frequency is usually small compared to the RF frequency. Each particle during acceleration describes in the longitudinal plane, an ellipse around the synchronous particle, as schematically represented in Fig. I.11.23.

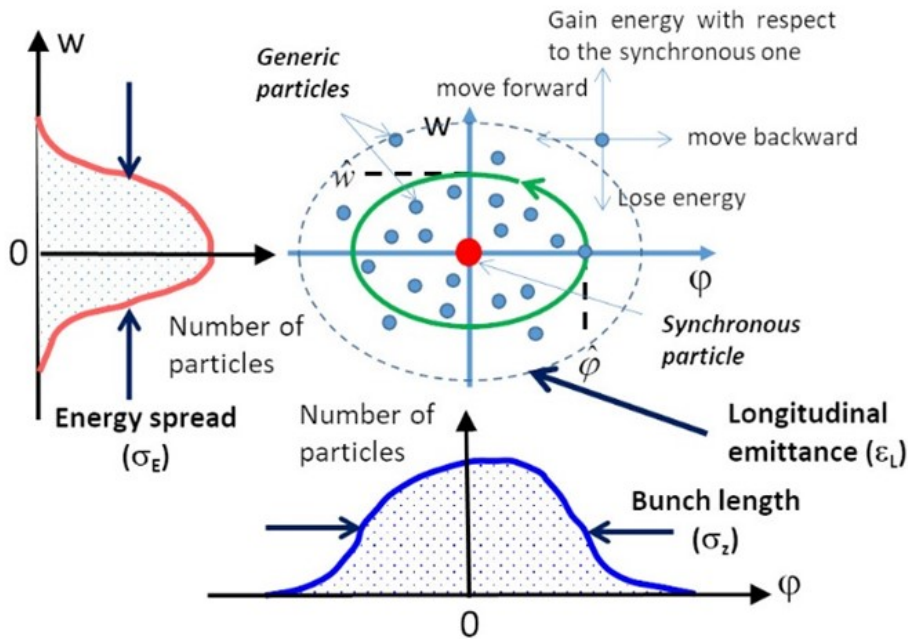


**Fig. I.11.23:** Oscillating particles in the longitudinal phase space around the synchronous one [10].

The maximum energy deviation is reached at  $\varphi = 0$  while the maximum phase excursion corresponds to  $w = 0$ . All particles in the bunch occupy an area in the longitudinal phase space called *longitudinal emittance* and the projections of the bunch in the energy and phase planes give the energy spread and the bunch length as schematically represented in Fig. I.11.23. From Eq. (I.11.56) it is also evident that the angular frequency  $\Omega_s$  scales with  $1/\gamma^{\frac{3}{2}}$ . This means that for ultra-relativistic electrons  $\Omega_T$  shrinks to zero and the beam is *frozen* and does not oscillate in the longitudinal plane.

#### I.11.10.4 Large-amplitude energy-phase oscillations

To study the longitudinal dynamics at large oscillations, we have to consider the non linear system of differential equations without the small-oscillation approximations (but still with the adiabatic acceleration approximation). It is easy to obtain (see Appendix II) that  $w$  and  $\phi$  satisfy the following relation

$$\frac{1}{2} \frac{\omega_{\text{RF}}}{c E_0 \beta_s^3 \gamma_s^3} w^2 + q \hat{E}_{\text{acc}} [\sin \phi - \phi \cos \phi_s] = \mathcal{H} \quad . \quad (\text{I.11.58})$$

This equation is basically the Hamiltonian of the system and the constant  $\mathcal{H}$  represent the total particle energy. Different values of  $\mathcal{H}$  gives different trajectories in the longitudinal phase space as reported in Fig. I.11.24. The oscillations are stable within a region bounded by a special curve called *separatrix*

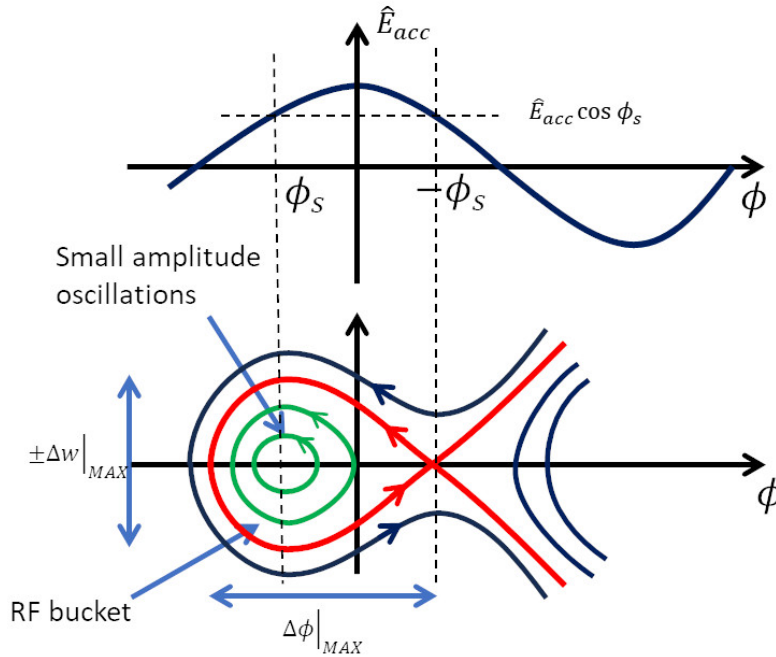


**Fig. I.11.24:** Oscillating particles in the longitudinal phase space around the synchronous one with indication of the separatrix curve (in red) [10].

whose equation is

$$\frac{1}{2} \frac{\omega_{\text{RF}}}{c E_0 \beta_s^3 \gamma_s^3} w^2 + q \hat{E}_{\text{acc}} [\sin \phi + \sin \phi_s - (\phi + \phi_s) \cos \phi_s] = 0 \quad . \quad (\text{I.11.59})$$

The region inside the separatrix is called the *RF bucket* and the trajectories outside the RF bucket are unstable. The dimensions of the bucket shrinks to zero if  $\phi_s = 0$ . The RF acceptance is defined as the maximum extension in phase and energy that we can accept in an accelerator. In particular the energy acceptance is given by

$$\pm \Delta w|_{\text{max}} = \pm 2 \left[ \frac{q c E_0 \beta_s^3 \gamma_s^3 \hat{E}_{\text{acc}} (\phi_s \cos \phi_s - \sin \phi_s)}{\omega_{\text{RF}}} \right]^{\frac{1}{2}} \quad . \quad (\text{I.11.60})$$

### I.11.10.5 Adiabatic phase damping

Equation (I.11.58) for small amplitude oscillations around the synchronous phase (see Appendix II) becomes

$$\frac{1}{2} \frac{\omega_{\text{RF}}}{c E_0 \beta_s^3 \gamma_s^3} w^2 - \frac{1}{2} q \hat{E}_{\text{acc}} \sin \phi_s \varphi^2 = \mathcal{H} \quad . \quad (\text{I.11.61})$$

This, as already pointed out in Section I.11.10.3, is the equation of an ellipse. A generic particle has its maximum energy deviation  $w_{\text{max}}$  when  $\varphi = 0$  and its maximum phase excursion  $\varphi_{\text{max}}$  when  $w = 0$  and then:

$$\begin{cases} w_{\text{max}} &= \left( \frac{2 c E_0 \beta_s^3 \gamma_s^3 \mathcal{H}}{\omega_{\text{RF}}} \right)^{\frac{1}{2}} \\ \varphi_{\text{max}} &= \left( -\frac{2 \mathcal{H}}{q \hat{E}_{\text{acc}} \sin \phi_s} \right)^{\frac{1}{2}} \end{cases} \quad . \quad (\text{I.11.62})$$

We can then rewrite Eq. (I.11.61) in the following form:

$$\frac{w^2}{w_{\text{max}}^2} + \frac{\varphi^2}{\varphi_{\text{max}}^2} = 1 \quad . \quad (\text{I.11.63})$$

It is possible to demonstrate that, since only conservative forces are present, the area of this ellipse remains constant during the acceleration, which means

$$A = \pi w_{\text{max}} \varphi_{\text{max}} = 2\pi \mathcal{H} \left( -\frac{\beta_s \beta_f^3 \gamma_f^3}{\Pi \hat{E}_{\text{acc}} \omega_{\text{RF}} \sin \phi_f} \right)^{\frac{\infty}{\epsilon}} = \text{constant} \quad . \quad (\text{I.11.64})$$

Assuming that the accelerating field and the synchronous phase are constant we have

$$\begin{cases} \varphi_{\text{max}} &\propto \frac{1}{(\beta_s \gamma_s)^{\frac{3}{4}}} \\ w_{\text{max}} &\propto (\beta_s \gamma_s)^{\frac{3}{4}} \end{cases} \quad . \quad (\text{I.11.65})$$

This means that, during acceleration, the bunch reduces its phase length and increases its energy spread (adiabatic phase damping). Concerning this last quantity it is important to remark that since the energy of the particle along the accelerator is proportional to  $\beta_s \gamma_s$  the relative energy spread also reduces.

### I.11.11 Longitudinal dynamics of low-energy electrons

From previous formulae it is clear that there is no motion in the longitudinal phase space for ultra-relativistic particles with  $\gamma \gg 1$ . This is the case of electrons, whose velocity is always close to the speed of light even at low energies. For electrons, accelerating structures are designed to provide an accelerating field synchronous with particles moving at  $v = c$ , as in the case of TW structures with phase velocity equal to  $c$ .

It is interesting to analyze what happens if we inject an electron beam generated in an electron gun (at low energy) directly in a TW structure (with  $v_{\text{ph}} = c$ ) and the conditions that allow to capture the beam<sup>2</sup> [41]. A sketch to depict this situation can be found in Fig. I.11.25.

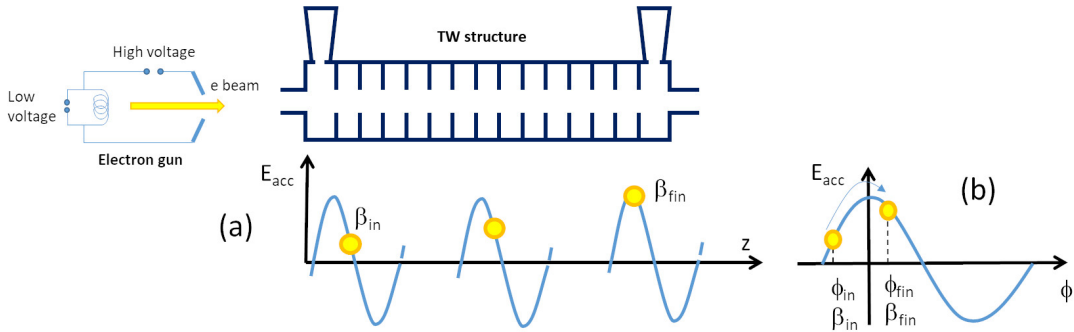


**Fig. I.11.25:** Basic scheme of a low-energy electron gun coupled with a TW accelerating structure: capture process (a) and phase slippage (b) [41].

Particles enter in the TW structure with velocity  $v < c$  and, initially, they are not synchronous with the accelerating field. In this part of the accelerator there is a *phase slippage*. After a certain distance the particles can reach enough energy (and velocity) to become synchronous with the accelerating wave (see Fig. I.11.25 (a)). This means that they are captured by the accelerator and, from this point on, they are permanently accelerated. If this does not happen (i.e. the energy increase is not enough to reach the velocity of the wave) they will be lost.

#### I.11.11.1 Phase slippage

We will now describe this phenomenon with a more precise mathematical approach. The accelerating field of a TW structure can be expressed by

$$E_{\text{acc}} = \hat{E}_{\text{acc}} \cos(\omega_{\text{RF}} t - kz) = \hat{E}_{\text{acc}} \cos \phi(z, t) \quad , \quad (\text{I.11.66})$$

where  $\phi$  represents the phase of the particle with respect to the accelerating wave. The equation of motion of a particle with a position  $z$  at time  $t$  accelerated by the TW is then, from the Lorentz force, given by

$$\frac{d(mv)}{dt} = \hat{E}_{\text{acc}} \cos(\phi(z, t)) \quad \Rightarrow \quad m_0 c \frac{d(\gamma \beta)}{dt} = m_0 c \gamma^3 \frac{d\beta}{dt} = q \hat{E}_{\text{acc}} \cos \phi \quad . \quad (\text{I.11.67})$$

<sup>2</sup>This is equivalent to consider instead of a TW structure a SW designed to accelerate ultra-relativistic particles at  $v = c$ . See Appendix I for the demonstration that the field in a multi-cell SW structure can be seen as the sum of two counter-propagating waves.

Integrating both terms of Eq. (I.11.67) between an initial and a final state [1, 38] we can find the relation between  $\beta$  and  $\phi$  from an initial condition to a final one

$$\sin \phi_{\text{fin}} = \sin \phi_{\text{in}} + \frac{2\pi E_0}{\lambda_{\text{RF}} q \hat{E}_{\text{acc}}} \left( \sqrt{\frac{1 - \beta_{\text{in}}}{1 + \beta_{\text{in}}}} - \sqrt{\frac{1 - \beta_{\text{fin}}}{1 + \beta_{\text{fin}}}} \right) . \quad (\text{I.11.68})$$

Supposing that the particle reaches, asymptotically, the value  $\beta_{\text{fin}} = 1$  we have

$$\sin \phi_{\text{fin}} = \sin \phi_{\text{in}} + \frac{2\pi m_0 c^2}{\lambda_{\text{RF}} q \hat{E}_{\text{acc}}} \sqrt{\frac{1 - \beta_{\text{in}}}{1 + \beta_{\text{in}}}} . \quad (\text{I.11.69})$$

Equation I.11.69 (or the more general Eq. (I.11.68)) gives several information on the physics of the low-energy acceleration process. First of all, in order to have a solution for the final phase  $\phi_{\text{fin}}$ , the second term of Eq. (I.11.69) should be in the interval  $[-1, 1]$ . This means that, for a given initial injection phase, we always have that  $\sin \phi_{\text{fin}} > \sin \phi_{\text{in}}$  that means  $\phi_{\text{fin}} > \phi_{\text{in}}$ . This is the mathematical description of the phase slippage phenomenon as represented in Fig. I.11.25(b). Another important consequence of Eq. (I.11.69) is that, for a given accelerating field and RF frequency, there are only some possible injection phases for which we can capture the beam. Conversely, for a given injection energy ( $\beta_{\text{in}}$ ) and phase  $\phi_{\text{in}}$  we can find the accelerating peak field ( $\hat{E}_{\text{acc}}$ ) which is necessary to have a relativistic beam at phase  $\phi_{\text{fin}}$ , necessary to capture the beam at phase  $\phi_{\text{fin}}$ .

### I.11.11.2 Bunch compression

Equation (I.11.69) is useful to describe the bunch compression during the capture process. As the injected beam moves up to the crest, in fact, it experiences also a longitudinal bunching, which is caused by velocity modulation (hence the name *velocity bunching*). This is evident plotting the final phases as a function of the injection phases for different accelerating field  $\hat{E}_{\text{acc}}$  as illustrated, for example, in Fig. I.11.26(a).

Differentiating Eq. (I.11.68) it is straightforward to derive the first order compression factor

$$\Delta \phi_{\text{fin}} = \Delta \phi_{\text{in}} \frac{\cos \phi_{\text{in}}}{\cos \phi_{\text{fin}}} . \quad (\text{I.11.70})$$

This mechanism can be used to compress the electron bunches in the first stages of acceleration [42].

### I.11.11.3 Capture efficiency and buncher

For a given  $E_{\text{acc}}$  we can easily calculate the range of the injection phases  $\phi_{\text{in}}$  actually accepted in the capture process (i.e. particles whose injection phases are within this range can be captured while the other are lost). Figure I.11.26 (b) illustrates this concept. Assuming an accelerating voltage of  $\hat{E}_{\text{acc}} = 17\text{MV/m}$  (and  $f_{\text{RF}} = 3\text{GHz}$ ), only the electrons that enter into the TW structure with a phase between  $-120$  and  $-60^\circ$  are captured, the other ones are lost. To reduce the number of lost particles there are, in principle, two possibilities. The first one is to increase the accelerating voltage, thus increasing the range of phases. The second one is to pre-shape the beam in order to increase the number of electrons that occupy the right phase interval. While the first solution requires more RF power to increase the accelerating field,

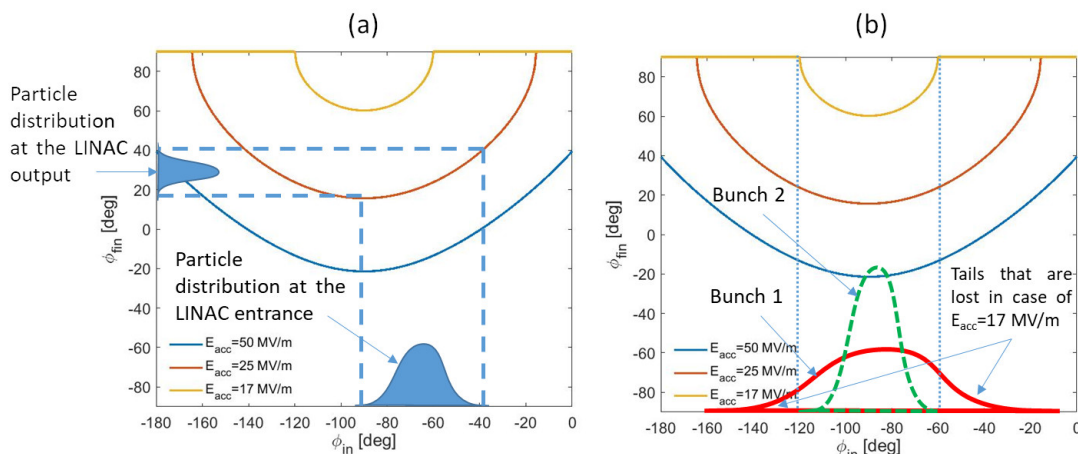


**Fig. I.11.26:** (a) Final phase as a function of the injection phase for different accelerating field, assuming  $f_{RF}=3$  GHz with two bunches sketched before and after the capture process; (b) Scheme of two bunches with different length captured by a TW structure coupled to a thermionic gun (the tails of the longer one are not captured by the low accelerating field) [10].

this second approach can be pursued with a simple scheme as illustrated in Fig. I.11.27, where a typical injector scheme is reported.

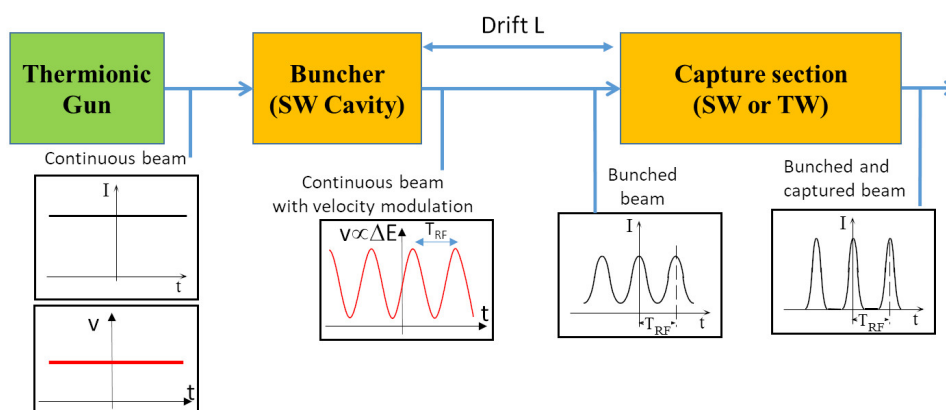


**Fig. I.11.27:** Scheme of a typical electron injector using a buncher [10].

This scheme foresees the use of a *buncher*. It is a SW cavity aimed at pre-forming the particle bunch gathering particles continuously emitted by a source by modulating the energy (and therefore the velocity) of the continuous emitted beam, using the longitudinal  $E$ -field of the SW cavity itself. After a certain drift space, the velocity modulation is “converted” to a density charge modulation. The density modulation depletes the regions corresponding to injection phase values incompatible with the capture process. The TW accelerating structure (capture section) is placed at an optimal distance from the buncher, to capture a large fraction of the charge and accelerate it up to relativistic energies. The amount of charge lost using this scheme is drastically reduced, while the capture section provides also further beam bunching.

### I.11.12 Transverse beam dynamics of accelerated particles

We will now describe more in detail the transverse motion of particles that are accelerated in a linac. The transverse beam dynamics is determined by the effect of the RF fields, by the magnetic elements (quadrupoles or solenoids) and by the collective effects such as space charge forces and wakefields [1].

#### I.11.12.1 RF transverse forces: defocusing term

The RF fields that accelerate particles act also on the transverse beam dynamics, because of the off axis transverse components of the electric and magnetic field, as schematically represented in Fig. I.11.28(a), which shows the electric field lines in a generic accelerating gap.

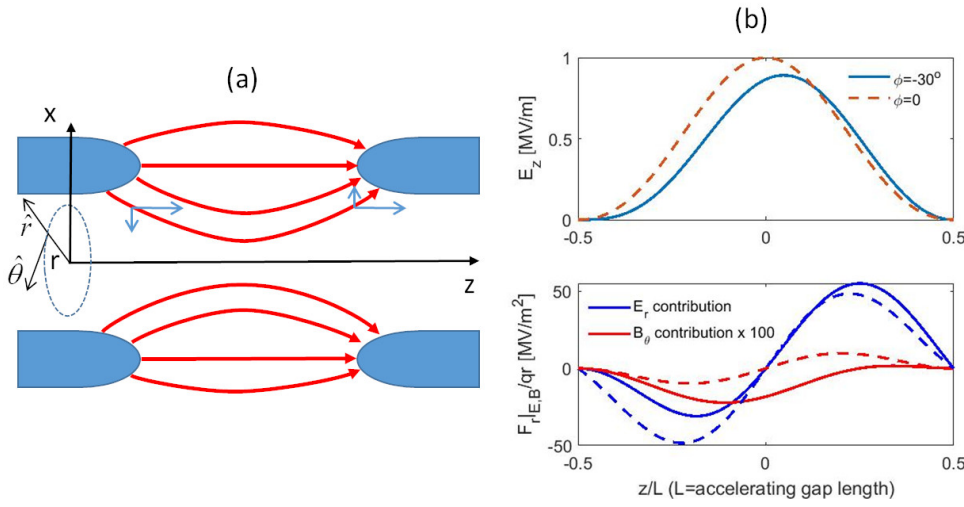


**Fig. I.11.28:** (a) Electric field lines in a generic accelerating gap; (b) transverse forces as a function of the longitudinal coordinate in traversing the accelerating gap.

More precisely, considering the Maxwell's equations in vacuum and assuming an accelerating SW field of the type reported in Eq. (I.11.10), we can calculate the transverse force

$$\begin{cases} \nabla \cdot \vec{E} & = 0 \\ \nabla \times \vec{B}, & = \frac{1}{c^2} \vec{E} \end{cases} \quad (\text{I.11.71})$$

or, in cylindrical coordinates,

$$\begin{cases} E_r & = -\frac{r}{2} \frac{\partial E_z}{\partial z} \\ B_\theta & = \frac{r}{2c^2} \frac{\partial E_z}{\partial t} \end{cases} \quad (\text{I.11.72})$$

Considering the Lorentz force

$$\frac{F_r}{q} = E_r - v B_\theta \quad , \quad (\text{I.11.73})$$

we now write the contribution of  $E$  and  $B$

$$\begin{cases} -\frac{r}{2} \frac{\partial E_{\text{RF}}(z)}{\partial z} \cos\left(\omega_{\text{RF}} \frac{z}{\beta c} + \phi_{\text{inj}}\right) & E \text{ contribution} \\ \frac{r}{2} \omega_{\text{RF}} \frac{\beta}{c} E_{\text{RF}}(z) \sin\left(\omega_{\text{RF}} \frac{z}{\beta c} + \phi_{\text{inj}}\right) & B \text{ contribution} \end{cases} \quad (\text{I.11.74})$$

As an example, the transverse forces as a function of the longitudinal coordinate are plotted in Fig. I.11.28(b) for an accelerating gap of  $L = 3$  cm, working at  $f_{\text{RF}} = 350$  MHz, for a  $\beta = 0.1$  and for two different injection phases. From the plot it is evident that the transverse forces are equal to zero in the center of the gap (except  $F_r|_B$  in the case  $\phi \neq 0$ ), while they have an opposite sign at the entrance and at the exit of the gap itself, as already visible in the schematic picture of Fig. I.11.28 (a). It is also evident that the electric field contribution is dominant and that, if the injection phase is negative (as required for longitudinal focusing) the two in/out contributions do not compensate, resulting in an integrated defocusing force.

Also for a multi-cell SW structure it is possible to calculate the transverse Lorentz force. The calculations can be found in Appendix III. In both cases it is possible to calculate the transverse momentum increase due to this RF transverse force. Assuming that the velocity and particle position do not change across the gap, we obtain to the first order

$$\Delta p_r = \int_{-L/2}^{+L/2} F_r \frac{dz}{\beta c} = -\frac{\pi q \hat{E}_{\text{acc}} L \sin \phi_{\text{inj}}}{c \gamma^2 \beta^2 \lambda_{\text{RF}}} r \quad , \quad (\text{I.11.75})$$

with  $\hat{E}_{\text{acc}}$  the average accelerating field and  $L$  the structure length.

The formula highlights the defocusing nature of such a term (since  $\sin \phi < 0$ ), that scales as  $1/\gamma^2$ . As a consequence, it disappears at relativistic regime (i.e. for electrons)<sup>3</sup>. For a correct evaluation of the defocusing effect in the non-relativistic regime we have also to take into account the velocity change across the accelerating gap, the transverse beam dimensions changes across the gap (with a general reduction of the transverse beam dimensions due to the focusing in the first part). Both contributions give a reduction of the defocusing force but the resulting one is still defocusing.

### I.11.12.2 RF focusing in electron linacs

We have pointed out that the RF defocusing term is negligible in electron linacs. It is important to mention that, for this type of linacs, there is a second order effect due to the non-synchronous harmonics of the accelerating field that give a net focusing contribution [43]. These harmonics generate a ponderomotive force, i.e. a force in an inhomogeneous oscillating electromagnetic field. As discussed in Ref. [43], it is possible to demonstrate that we have an average focusing force given by this expression

$$\bar{F}_r = -rq \frac{\hat{E}_{\text{acc}}^2}{8\gamma \frac{m_0 c^2}{e}} \eta(\varphi) \quad , \quad (\text{I.11.76})$$

where the term  $\eta(\varphi)$  is a factor that depends on the harmonic content of the accelerating field and is of the order of 0.1 [43]. This harmonic content is larger in SW cavities because of the presence of the wave that propagates in the opposite direction with respect to the beam (as pointed out in Appendix I and III). With accelerating gradients of few tens of MV/m it is quite easy to verify that this transverse gradient can easily reach the level of MV/m<sup>2</sup>. In Appendix IV, the derivation of the ponderomotive force is illustrated with a particular application to the case of a multi cell SW structure.

<sup>3</sup>In the case of electrons, moreover, we already pointed out that, in general,  $\phi = 0$  for maximum acceleration and this also cancel the defocusing effect.

### I.11.12.3 Collective effects: space charge forces

Collective effects are phenomena related to the number of particles in a bunch, and, in linacs, they can play a crucial role in the longitudinal and transverse dynamics of intense beams. They are typically related to space charge effects and wakefield but here we will focus only on the former. This effect is generated by the Coulomb repulsion between particles. If we consider a uniform and infinite cylinder of charge with radius  $R_b$  moving along the longitudinal axis  $z$  with an average current  $I$ , it is quite easy to verify that the force experienced by a generic particle inside the cylinder at a radius  $r_q$  is given by

$$\vec{F}_{SC} = q \frac{I}{2\pi \epsilon_0 R_b^2 \beta c \gamma^2} r_q \hat{r} \quad . \quad (\text{I.11.77})$$

This simple example give us a couple of interesting informations: the effect of space charge is of particular concern for low energy particles and high currents, because the space charge forces scale as  $\frac{1}{\beta \gamma^2}$  and linearly with the current  $I$ . In this particular example the force is linear with the displacement  $r_q$ , but in general space charge forces are non-linear and depend on the beam particle distribution.

### I.11.12.4 Magnetic focusing, transverse oscillations and $\beta$ -function

In the previous paragraphs we pointed out that the RF and space charge forces (or the natural divergence of the beam given by a generic source) give a defocusing effect and need to be compensated, in order to take under control, the transverse beam dynamics in a linac. For this reason, quadrupoles are used to focus the beam and, at low energies, also solenoids. We will consider, in particular, the first type of elements. As done in all accelerator machines with strong focusing magnets, quadrupoles are used in an alternating configuration, since they are focusing in one plane and defocusing into the other. In a linac they are interleaved by either accelerating gaps or accelerating structures. The type of magnetic configuration and the magnets distance depend on the type of particles, energy, beam intensity and beam dimensions requirements. Due to the alternating quadrupole focusing system, each particle (as in synchrotrons) performs transverse oscillations and the equation of motion in the transverse plane is of the type

$$\frac{d^2x}{ds^2} + K^2(s)x - F_{SC} = \frac{d^2x}{ds^2} + [k^2(s) - k_{RF}^2(s)]x - F_{SC} = 0 \quad , \quad (\text{I.11.78})$$

where the  $K(s)$  term takes into account the magnetic focusing configuration  $k(s)$  and the RF defocusing effect  $k_{RF}(s)$  that exhibits a linear behavior with the particle displacement, while the  $F_{SC}$  term is the non-linear space charge term.

If we neglect the space charge forces and we assume  $K^2 > 0$ , the solution of the single particle trajectory described by the Eq. (I.11.78) is a pseudo-sinusoid described by the equation<sup>4</sup>

$$x(s) = \sqrt{\epsilon_0 \beta(s)} \cos \left[ \int_{s_0}^s \frac{ds}{\beta(s)} + \varphi_0 \right] \quad , \quad (\text{I.11.79})$$

where the characteristic  $\beta$ -function depends on the magnetic and RF configuration along the linac and the constants  $\epsilon_0$  and  $\varphi_0$  depend on the initial conditions of the particle at the entrance of the linac (i.e. position

<sup>4</sup>Unfortunately, here we use the Twiss function  $\beta$  (for which we use a slightly different font) that has the same notation than the relativistic factor  $\beta$ . They are, obviously, two completely different quantities.

and angle). Figure I.11.29 (a) shows, as an example, different particle trajectories corresponding to different initial conditions. It is quite easy to verify that, because of Eq. (I.11.79), all particles oscillations are contained within an envelope that scales with the square root of the  $\beta$ -function and also the final transverse beam dimensions  $\sigma_{x,y}(s)$  vary along the linac within the same envelope.

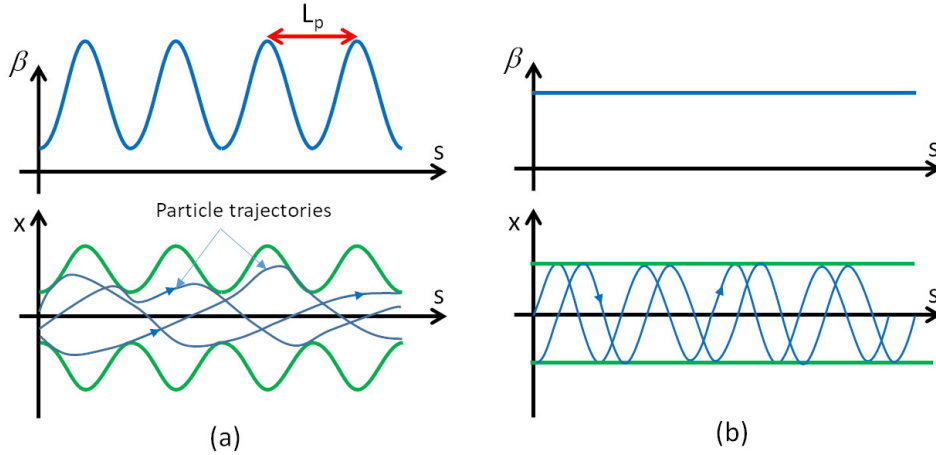


**Fig. I.11.29:** (a) Sketch of the  $\beta$ -function and transverse particle trajectories along the linac; (b)  $\beta$ -function and transverse particle trajectories in the case of *smooth approximation*.

Because of the regular magnetic and accelerating structure configuration, the  $\beta$ -function is “locally” periodic, and it is useful to refer to the focusing period ( $L_p$ ) that is the length after which the focusing structure is repeated (usually equal to  $N \beta\lambda$ ). The transverse phase advance per period is defined as

$$\sigma = \int_{L_p} \frac{ds}{\beta(s)} \approx \frac{L_p}{\langle \beta \rangle} \quad , \quad (\text{I.11.80})$$

where  $\langle \beta \rangle$  is the average  $\beta$  in the focusing period. For transverse oscillation stability,  $0 < \sigma < \pi$  should be in the range  $0 < \sigma < \pi$  [1]. The quantity  $\sigma/L_p$  is called phase advance per unit length.

### I.11.12.5 Smooth approximation of the transverse oscillations

In case of *smooth approximation* of the linac, we consider the average effect of the quadrupoles and RF and, as a consequence, a constant  $\beta$ -function. Assuming a focusing structure of the type sketched in Fig. I.11.30, which alternates focusing quadrupoles with accelerating gaps (also called a FODO lattice) we obtain a simple harmonic motion along the  $s$  coordinate of the type

$$x(s) = \sqrt{\epsilon_0} \sqrt{\frac{1}{K_0}} \cos(K_0 s + \varphi_0) \quad . \quad (\text{I.11.81})$$

In particular for this simple case, we obtain that the phase advance per unit length  $K_0$  is equal to [1]

$$K_0 = \sqrt{\underbrace{\left( \frac{q G l}{2 m_0 c \gamma \beta} \right)^2}_{\text{magnetic focusing}} - \underbrace{\frac{\pi q \hat{E}_{\text{acc}} \sin(-\phi)}{m_0 c^2 \lambda_{\text{RF}} (\gamma \beta)^3}}_{\text{RF defocusing}}} \quad (\text{I.11.82})$$

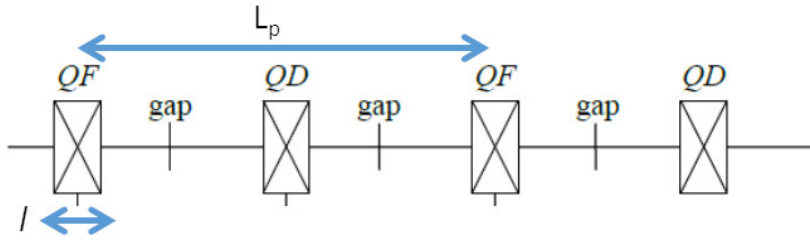


**Fig. I.11.30:** Focusing structure considered in the smooth approximation (FODO lattice).

where  $G$  [T/m] is the quadrupole gradient,  $l$  [m] is the quadrupole length, and all the other quantities have been already defined in the previous sections (note that  $\beta$  in this formula is the relativistic factor). In this last formula it is possible to recognize the two contributions of the *magnetic focusing* and of the *RF defocusing* which appear with opposite signs. This simplified approach allows to make several considerations. First of all, the RF defocusing term scales with  $f_{\text{RF}}$  ( $1/\lambda_{\text{RF}}$ ), and this sets the upper limit to the working frequency of the cavities (i.e., at lower particle energies, it is better to operate at a lower frequency). Moreover, as already pointed out, the RF defocusing term plays a crucial role at low energy, since the defocusing term scales as  $1/(\gamma\beta)^3$ . If we consider also the space charge contribution and the simple case of an ellipsoidal beam of charge  $Q$  (that generates linear space charge forces) we obtain for  $K_0$  the following expression [1]

$$K_0 = \sqrt{\left(\frac{q G l}{2 m_0 c \gamma \beta}\right)^2 - \frac{\pi q \hat{E}_{\text{acc}} \sin(-\phi)}{m_0 c^2 \lambda_{\text{RF}} (\gamma \beta)^3} - \underbrace{\frac{3 Z_0 q I \lambda_{\text{RF}} (1-f)}{8 \pi m_0 c^2 \beta^2 \gamma^3 r_x r_y r_z}}_{\text{space charge defocusing}}}, \quad (\text{I.11.83})$$

where  $I$  is the average beam current ( $= Q/T_{\text{RF}}$ ),  $r_x$ ,  $r_y$ ,  $r_z$  are the ellipsoid semi-axes,  $f$  is a form factor ( $0 < f < 1$ ) and  $Z_0$  is the free space impedance (equal to  $377 \Omega$ ). For ultra-relativistic particles (e.g., electrons of several MeV) both the RF defocusing and the space charge terms disappear and the external focusing remains to control the emittance and beam dimensions and to stabilize the beam against instabilities.

#### I.11.12.6 General considerations on linac optics design for protons and ions

For protons and ions, according to what has been illustrated, the beam dynamics is completely dominated by space charge and RF defocusing forces. Focusing is usually provided by quadrupoles that are also integrated in the drift tubes of DTL structures. The phase advance per period ( $\sigma$ ) should be, in general, in the range  $30$ - $80^\circ$  [1,2]. This means that, at low energy, we need a strong focusing term (short quadrupole distance and high quadrupole gradient) to compensate for the RF defocusing, but the limited space in the drift tubes (proportional to  $\beta \lambda$ ) limits this achievable integrated gradient and, as a consequence, the beam current. As  $\beta$  increases, the distance between focusing elements can increase:  $\beta \lambda$  in the DTL goes, as example, from  $\sim 70$  mm at 3 MeV,  $f_{\text{RF}} = 350$  MHz to  $\sim 250$  mm at 40 MeV and can be increased to  $4$ - $10 \beta \lambda$  at higher energy ( $> 40$  MeV). As already pointed out, the overall linac is made of a sequence of structures, matched to the beam velocity, and where the length of the focusing period increases with

energy. As  $\beta$  increases, longitudinal phase error between cells of identical length becomes small, and we can have short sequences of identical cells (instead of cells all with different dimensions) with a reduction of the overall construction costs. From beam dynamics simulations it is possible to calculate the beam radius along the structures which in turn allows to calculate the margin between beam radius and physical apertures.

#### I.11.12.7 General considerations on linac optics design for electrons

For electrons, space charge forces act only at low energy or high peak current. Below 10-20 MeV (injector) the beam dynamics optimization has to include emittance compensation schemes using, typically, solenoids. At higher energies, no space charge and no RF defocusing effects occur, but we have RF focusing due to the ponderomotive force in accelerating structures. In this section of the linac focusing periods up to several metres can occur. Nevertheless, the optics design has to take into account longitudinal and transverse wakefields (due to the higher frequencies used for acceleration) that can cause energy spread increase, head-tail oscillations and multi-bunch instabilities. For the longitudinal bunch compression schemes based on magnets and chicanes one has also to take into account, in the case of short bunches, the interaction between the beam and the emitted synchrotron radiation in bending magnets (Coherent Synchrotron Radiation effects CSR) [44, 45]. All these effects are important especially in linacs for Free Electron Lasers (FEL) that require extremely good beam qualities, short bunches and high-peak current.

#### I.11.13 Radio Frequency quadrupoles (RFQ)

At low proton (or ion) energies ( $\beta \sim 0.01$ ), space charge defocusing is strong and quadrupole focusing is not very effective (because of the low  $\beta$ ). Moreover, cell lengths become small and conventional accelerating structures (DTL) are very inefficient. At these energies, one may use another type of structure, called Radio Frequency Quadrupole (RFQ), invented in the '60 by Kapchinskiy and Tepliakov [46]. These structures allow to simultaneously provide transverse focusing, acceleration and bunching of the beam. A sketch of the structure and the picture of one are shown in Fig. I.11.31.

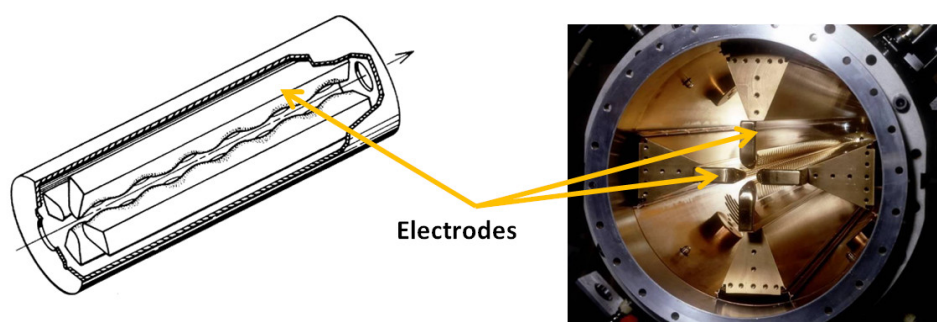


**Fig. I.11.31:** Sketch and picture of a RFQ structure.

The transverse focusing effect is due to the fact that the resonating mode of the cavity (between the four electrodes) is the quadrupole mode  $TE_{210}$ , whose electric field lines are shown in Fig. I.11.32 (a). The working principle of a quadrupole electric mode is similar to that of a magnetic quadrupole with

no field in the center of the structure and a transverse electric field that increases linearly with beam off-axis and that is focusing in one plane and defocusing in the other. The RF alternating voltage on the electrodes produces an alternating focusing channel with a period RF.

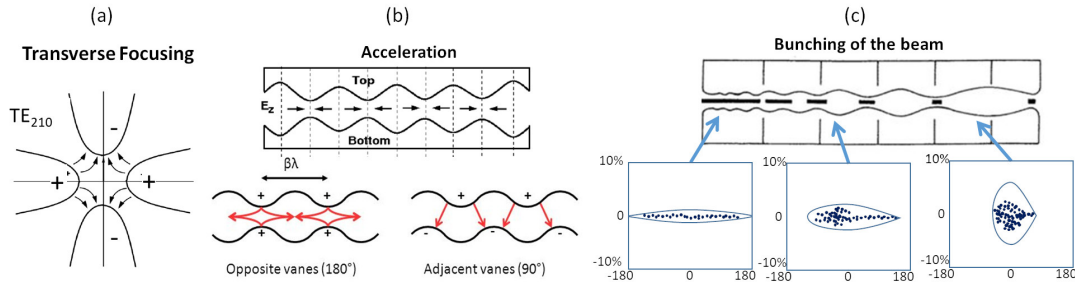


**Fig. I.11.32:** (a) Quadrupole mode ( $TE_{210}$ ) of the RFQ four vane geometry; (b) Longitudinal modulation of the electrodes and indication of the electric field lines; (c) Bunching mechanism in RFQ.

The acceleration process is achieved by means of a longitudinal modulation of the vanes with period  $\beta\lambda_{RF}$ . This creates a longitudinal component of the electric field (as given in Fig. I.11.32 (b)) that accelerates the beam (the modulation corresponds exactly to a series of RF gaps).

The third effect, i.e. the bunching, is obtained by changing the modulation period (distance between electric field maxima), since it is designed to change the phase of the beam with respect to the RF field during beam acceleration, while the amplitude of the modulation can be varied to change the accelerating gradient. The continuous beam enters the first cell and it is bunched around the  $-90^\circ$  phase (bunching cells), progressively the beam is bunched and accelerated (adiabatic bunching channel) and, only in the last cells we have a switch to a pure acceleration process. The process is illustrated in Fig. I.11.32 (c). The mathematical description of this process would require a dedicated course and is out of the scope of the present proceeding. Details can be found in Refs. [1, 47].

#### I.11.14 Choice of the frequency of operation and accelerating structures

The choice of the frequency and type of accelerating structures depends on several factors such as:

- Type of particles to be accelerated,
- Average beam current and duty cycle,
- Available space and compactness,
- Cost.

Table I.11.1 schematically illustrates how the accelerating structure parameters scale with frequency [20].

For NC structures  $r$  increases with frequency as  $f^{1/2}$  and this forces to adopt higher frequencies. Nevertheless, at high frequencies the beam-cavity interaction due to wakefields becomes more critical ( $w_z \propto f^2$ ,  $w_\perp \propto f^3$ ). On the other hand, for SC structures it can be demonstrated that the power losses increase with  $f^2$  and, as a consequence,  $r$  scales with  $1/f$ , and this forces to adopt lower frequencies.

**Table I.11.1:** Scaling laws for cavity parameters with frequency.

Parameter	NC	SC
Surface resistance ( $R_s$ )	$\propto f^{1/2}$	$\propto f^2$
Quality factor ( $Q$ )	$\propto f^{-1/2}$	$\propto f^{-2}$
Shunt impedance per unit length ( $r$ )	$\propto f^{1/2}$	$\propto f^{-1}$
$r/Q$		$\propto f$
Longitudinal wakefield ( $w_z$ )		$\propto f^2$
Transverse wakefield ( $w_\perp$ )		$\propto f^3$

Higher frequencies allow to achieve, in general, higher accelerating gradients in NC structures but require higher mechanical precision in the fabrication of the structures. Moreover, at very high frequencies (>10-12 GHz) power sources are either commercially not available or very expensive. On the other hand, at low frequencies one needs more bulk material and machines have generally a larger footprint.

In DTL, for protons and ions, the accelerating cell dimensions (that scale as  $\sim c\beta/f_{\text{RF}}$ ) are not practical at high frequency (as example at 3 GHz and  $\beta=0.1$  the accelerating cells are 10 mm), besides the insertion of magnetic elements in the drift tubes for transverse focusing is not possible. Also, the RF defocusing effects scale as  $1/f$  and they do not allow a stable acceleration of the beam.

In general, a given accelerating structure has a curve of efficiency (shunt impedance per unit length) with respect to the particle energy and, if it works at given  $\beta$ , the same structure, becomes not efficient at larger  $\beta$  and the transition to another type of structure is necessary.

As a general consideration, normal conducting linacs require high peak power from power sources and also high average power in case of operation at relatively high DC (0.1-1%). For high duty cycle linacs (> 1%) the use of superconducting structures is the only possible solution.

Given all previous reviews, it is possible to make some general considerations schematically reported in Table I.11.2.

**Table I.11.2:** Typical use of different accelerating structures (not exhaustive).

Cavity Type	$\beta$ Range	Frequency	Particles Type
RFQ	0.01– 0.1	40-500 MHz	Protons, Ions
DTL	0.05 – 0.5	100-500 MHz	Protons, Ions
Multi cell ( $\pi$ or $\pi/2$ cavities)	0.5 – 1	600 MHz-3 GHz	Protons, Electrons
SC multi cell $\pi$ -mode	> 0.5-1	350 MHz-3 GHz	Protons, Electrons
TW	1	3-12 GHz	Electrons

In low duty cycle ( $< 10^{-3}$ ) electron linacs, higher frequencies (up to the X band) can be used for both SW and TW structures. Proton and ion linacs use low frequencies (40-500 MHz) up to  $\beta \sim 0.5$  with RFQ or DTL structures. At higher energies ( $\beta > 0.5$ ) SW multi cell structures at higher operating frequencies are used (from 500 MHz up to few GHz).

Superconducting multi cell cavities working on the  $\pi$ -mode, are used in high duty cycle linacs

starting from  $\beta$  larger than 0.5 and, in case of protons or ions, combined with low frequency structures in the first stages of acceleration. A complete review of superconducting accelerating cavities is given in [48].

### I.11.15 Collection of exercises

#### I.11.15.1 EXERCISE 1: TRANSIT TIME FACTOR

1. Derive the general expression of the transit time factor of an accelerating gap of length  $L$ , with constant accelerating field, in which the field is oscillating at  $f_{\text{RF}}$  and that accelerates particles with relativistic factor  $\beta$ .
2. Remembering that the light wavelength in free space is given by  $\lambda_{\text{RF}} = c/f_{\text{RF}}$ , for which value of the accelerating gap length  $L$ ,  $T$  is equal to zero?
3. Calculate the numerical value of  $T$  for  $L = 10$  cm,  $f_{\text{RF}} = 1$  GHz and ultra-relativistic electrons ( $\beta = 1$ ).
4. Calculate the accelerating voltage as a function of the gap length  $L$  assuming an injection phase on crest ( $\phi_{\text{inj}} = 0$ ) and for which value of the gap length his value is maximum. Calculate the numerical value assuming  $\beta = 0.5$  and  $f_{\text{RF}} = 400$  MHz.

#### I.11.15.2 EXERCISE 2: ALVAREZ STRUCTURES

A proton beam is injected into a DTL (Alvarez structure) working at  $f_{\text{RF}} = 300$  MHz, with a kinetic energy  $W_{\text{in}} = 4$  MeV.

1. Calculate the distance between the first two centers of the accelerating gaps ( $L_{\text{gaps}}$ ) assuming a constant velocity of the proton beam between the first two gaps and a negligible increase of the velocity due to the accelerating field.
2. If the structure is composed by 40 accelerating gaps ( $N_{\text{gaps}}$ ) and the average accelerating voltage per gap is  $V_{\text{acc}} = 0.5$  MV, calculate the final proton beam kinetic energy.

(Proton rest energy:  $m_{0,p} c^2 = E_{0,p} = 938$  MeV, velocity of light  $c = 2.998 \times 10^8$  m/s)

#### I.11.15.3 EXERCISE 3: FILLING TIME SW CAVITY

A SW cavity is fed by an RF generator with constant power, calculate after how much time the field in the cavity is 90% of the field at full regime supposing that the cavity operates at  $f_{\text{RF}} = 1.3$  GHz and has an equivalent  $Q$  factor of 10000.

#### I.11.15.4 EXERCISE 4: $\pi$ -MODE STRUCTURES

A  $\pi$ -mode structure, operating at  $f_{\text{RF}} = 400$  MHz, is made up of  $N = 8$  cells and is used to accelerate protons. Each single cell has a shunt impedance  $R = 3$  M $\Omega$  and a length  $L_{\text{cell}} = 15$  cm. Calculate:

1. The total shunt impedance of the  $\pi$ -mode structure;
2. The accelerating voltage if the total dissipated power into the cavity is  $P_{\text{diss}} = 1$  MW;
3. The average accelerating field;
4. The average  $\beta$  of the proton beam accelerated by this structure.

#### I.11.15.5 EXERCISE 5: TW STRUCTURES PARAMETERS

Considering a generic constant impedance TW structure, demonstrate that:

1. Having defined the attenuation constant as  $\alpha = p_{\text{diss}}/(2 P_F)$  the power flow along the structure scales as

$$P_F(z) = P_{\text{in}} e^{-2\alpha z} \quad ,$$

where  $P_{\text{in}}$  is the structure input power.

2. Having defined the shunt impedance per unit length as

$$r = \frac{\hat{E}_{\text{acc}}^2}{p_{\text{diss}}} \quad ,$$

the accelerating field sampled by an ultra-relativistic particle ( $z = ct$ ) along the structure can be expressed as

$$\hat{E}_{\text{acc}}(z) = \sqrt{2\alpha r P_{\text{in}}} e^{-\alpha z} = E_{\text{in}} e^{-\alpha_0 z} \quad .$$

3. The total accelerating voltage is given by

$$\hat{V}_{\text{acc}} = E_{\text{in}} \frac{1 - e^{-\alpha L}}{\alpha} \quad .$$

4. The group velocity defined as the velocity of the propagation the electromagnetic energy in the structure is given by

$$v_g = \frac{P_F}{w} \quad .$$

#### I.11.15.6 EXERCISE 6: TW STRUCTURES

A SLAC-type TW structure accelerates ultra-relativistic electrons. The structure length is  $L = 3$  m and it can be simplified as a structure with a group velocity  $v_g = 1.1\%$  of the velocity of light.

1. Calculate the filling time;
2. If we suppose that the structure has a field attenuation constant  $\alpha = 0.2 \text{ m}^{-1}$ , calculate the total accelerating voltage if the accelerating field at the beginning of the structure is  $E_{\text{in}} = 20$  MV/m;
3. Calculate the average accelerating field;

4. If the average dissipated power per unit length in the structure, corresponding to the previous value of the accelerating field, is  $p_{\text{diss}} = 4 \text{ MW/m}$  calculate the shunt impedance per unit length.

#### I.11.15.7 EXERCISE 7: $\pi$ -MODE STRUCTURES AND DUTY CYCLE

A multi-cell SW cavity, operating on the  $\pi$ -mode at 1 GHz, accelerates protons at  $\beta = 0.5$ . The cavity is a 9-cell structure. Assuming a negligible variation of the particle velocity through the cavity itself:

1. Calculate the distance between the centers of the accelerating cells;
2. Assuming a shunt impedance of the single cell  $R$  of  $1 \text{ M}\Omega$ , calculate the dissipated power to have an effective accelerating voltage on the overall structure of  $V_{\text{acc}} = 10 \text{ MV}$ ;
3. Calculate the average accelerating field.
4. If the cavity is fed by  $4 \mu\text{s}$  RF pulses with a repetition rate of 100 Hz, calculate the Duty Cycle.

#### I.11.15.8 EXERCISE 8: ENERGY ACCEPTANCE

A RF accelerating structure operating at  $f_{\text{RF}} = 400 \text{ MHz}$ , is used to accelerate protons at an input nominal kinetic energy  $W_{\text{in}} = 10 \text{ MeV}$ . Assuming that the nominal synchronous phase  $\phi_s = -\pi/6$  and that the average accelerating field is  $E_{\text{acc}} = 2 \text{ MV/m}$ , calculate the maximum kinetic energy of the protons that is possible to capture in the RF bucket (assuming that it is injected at a phase corresponding to the synchronous one).

#### I.11.15.9 EXERCISE 9: ENERGY ACCEPTANCE AND LONGITUDINAL PHASE ADVANCE

A 400 MHz DTL accelerates protons with an injection energy of 2.5 MeV.

1. If we want to accept particles with a relatively energy spread at injection of  $\pm 5\%$ , what is the average accelerating field if the synchronous phase is  $\phi_s = -30^\circ$ ?
2. What is the longitudinal phase advance per meter at injection and after 10 meters?
3. If the bunch length at the input of the structure is 5 cm, what is its bunch length after 10 meters?

#### I.11.15.10 EXERCISE 10: LOW ENERGY ELECTRONS

An electron beam generated by a DC gun at 40 keV is directly accelerated by a TW structure.

1. Calculate the minimum accelerating field needed to capture the beam, assuming an operating frequency of 6 GHz and a final  $\beta_{\text{fin}}$  equal to 1.
2. If the accelerating field is twice the minimum accelerating field, what is the final phase  $\phi_{\text{fin}}$  with respect to the accelerating field of a particle injected at  $\phi_{\text{in}} = -\pi/2$ ?

**I.11.15.11 EXERCISE 11: TRANSVERSE BEAM DYNAMICS**

A DTL (Alvarez structure) working at  $f_{RF} = 300$  MHz accelerates protons with an injection energy  $W_{in} = 4$  MeV, permanent magnet quadrupoles are inside the drift tubes and the focusing system is equivalent to a FODO lattice, as sketched below. The quadrupoles inside the drift tubes have a length  $L_Q = 5$  cm.

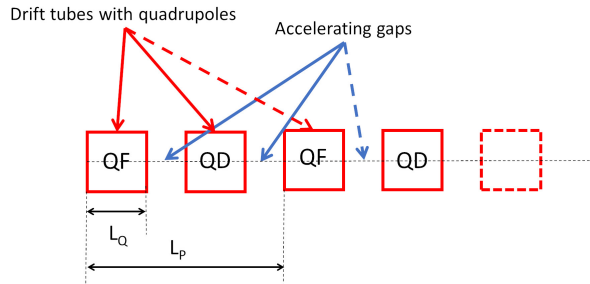


**Fig. I.11.33:** Ex. 11 FODO schematics.

If the average accelerating field per cell is  $E_{acc} = 2$  MV/m and the nominal synchronous phase  $\phi_s = -\pi/6$ , calculate, using the **smooth approximation** approach, the quadrupole gradient ( $G$ ) that is necessary to have, in the first cells, of the structure in order to achieve a **transverse phase advance per period ( $\sigma$ ) equal to  $\pi/3$** , supposing that the period of the FODO ( $L_P$ ) is exactly twice the distance between two accelerating gaps.

**I.11.15.12 EXERCISE 12: TRANSVERSE BEAM DYNAMICS - II**

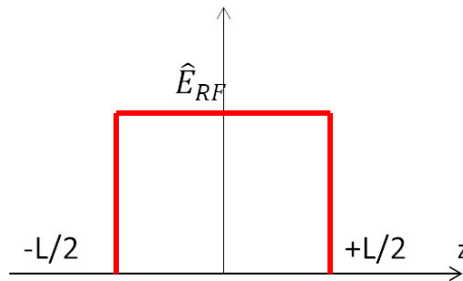
A proton beam is injected into a DTL Alvarez structure working at  $f_{RF} = 300$  MHz, with a kinetic energy  $W_{in} = 10$  MeV. The transverse focusing is performed with a FODO structure using permanent magnet quadrupoles with  $G = 50$  T/m inside the drift tubes that have an equivalent magnetic length  $L_Q = 8$  cm. The average accelerating field per cell is  $E_{acc} = 2$  MV/m and the nominal synchronous phase  $\phi_s = -\pi/4$ .

Calculate, in **smooth approximation**, the average transverse  $\beta$ -function required to obtain an ellipsoidal beam with an average beam current  $I = 20$  mA, and beam radii  $r_x = r_y = 1$  mm and  $r_z = 5$  mm assuming a form factor  $f = 0.5$ .

**I.11.16 Solutions to the exercises**
**I.11.16.1 EXERCISE 1: TRANSIT TIME FACTOR**

1. Considering the uniform field distribution reported below and the definition of the transit time factor of Eq. I.11.6 we have

$$\begin{aligned}
 T &= \frac{\int_{-L/2}^{L/2} E_{\text{RF}}(z) \cos\left(\omega_{\text{RF}} \frac{z}{v}\right) dz}{\int_{-L/2}^{L/2} E_{\text{RF}}(z) dz} \\
 &= \frac{\int_{-L/2}^{L/2} \cos\left(\omega_{\text{RF}} \frac{z}{\beta c}\right) dz}{L} \\
 &= \frac{\sin\left(\omega_{\text{RF}} \frac{L}{2\beta c}\right)}{\frac{\omega_{\text{RF}} L}{2\beta c}} = \frac{\sin\left(\frac{\pi L}{\beta \lambda_{\text{RF}}}\right)}{\frac{\pi L}{\beta \lambda_{\text{RF}}}} \quad .
 \end{aligned} \tag{I.11.84}$$



2. The previous expression is equal to zero when

$$2\pi f_{\text{RF}} \frac{L}{2\beta c} = \frac{\pi L}{\beta \lambda_{\text{RF}}} = \pi \quad \Rightarrow \quad L = \beta \lambda_{\text{RF}} \quad .$$

- 3.

$$T = \frac{\sin\left(\pi \cdot 1 \cdot 10^9 \frac{0.1}{3 \cdot 10^8}\right)}{\pi \cdot 1 \cdot 10^9 \frac{0.1}{3 \cdot 10^8}} \sim 0.8268 \quad .$$

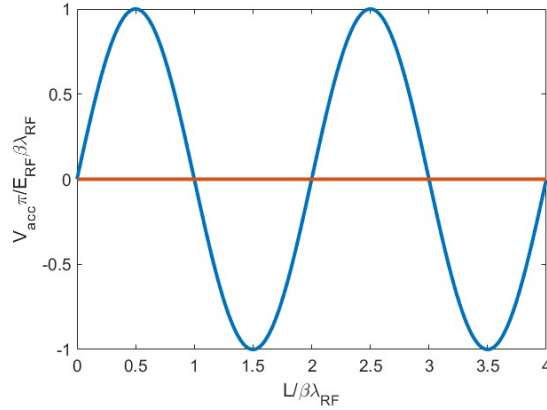
- 4.

$$\begin{aligned}
 \hat{V}_{\text{acc}} &= \int_{-L/2}^{L/2} E_{\text{RF}}(z) dz \left[ \frac{\sin\left(\frac{\pi L}{\beta \lambda_{\text{RF}}}\right)}{\frac{\pi L}{\beta \lambda_{\text{RF}}}} \right] \\
 &= \hat{E}_{\text{RF}} L \frac{\sin\left(\frac{\pi L}{\beta \lambda_{\text{RF}}}\right)}{\frac{\pi L}{\beta \lambda_{\text{RF}}}} \quad . \\
 &= \hat{E}_{\text{RF}} \frac{\sin\left(\frac{\pi L}{\beta \lambda_{\text{RF}}}\right)}{\frac{\pi}{\beta \lambda_{\text{RF}}}}
 \end{aligned}$$

The plot of the accelerating voltage is reported below. The maximum accelerating voltage is obtained when

5.

$$\hat{V}_{\text{acc}} |_{\text{max}} \rightarrow \frac{L}{\beta \lambda_{\text{RF}}} = \frac{1}{2} \Rightarrow L = \frac{\beta \lambda_{\text{RF}}}{2} = \frac{\beta c}{2 f_{\text{RF}}} .$$



The optimum gap length scales linearly with the  $\beta$  of the particles. To calculate the numerical value it is enough to substitute in the previous formula the numbers

$$L = \frac{\beta c}{2 f_{\text{RF}}} = 18.7 \text{ cm}.$$

### I.11.16.2 EXERCISE 2: ALVAREZ STRUCTURES

1. From the relation  $L_n = \bar{\beta}_n \lambda_{\text{RF}}$  we obtain  $L_{\text{gaps}} = \beta_{\text{in}} \lambda_{\text{RF}} = 92 \text{ mm}$ .

Having  $\lambda_{\text{RF}} = c / f_{\text{RF}} = 0.9993 \text{ m}$

$\gamma_{\text{in}} = (W_{\text{in}} + E_{0,p}) / E_{0,p} = 1.0043$

$\beta_{\text{in}} = \sqrt{1 - 1/\gamma_{\text{in}}^2} = 0.0921$

2. The final kinetic energy is given by  $W_{\text{fin}} = W_{\text{in}} + q N_{\text{gaps}} V_{\text{acc}} = 24 \text{ MeV}$ .

### I.11.16.3 EXERCISE 3: FILLING TIME SW CAVITY

The accelerating voltage increase exponentially and we have that

$$V_{\text{acc}}(t_{90\%}) = \hat{V}_{\text{acc}} \left( 1 - e^{-\frac{t_{90\%}}{\tau_F}} \right) = 0.9 \hat{V}_{\text{acc}} .$$

Remembering that the filling time for a SW cavity is given by

$$\tau_F = \frac{2Q}{\omega_{RF}} = \frac{2 \cdot 10000}{2\pi \cdot 1.3 \cdot 10^9} = 2.45 \mu\text{s} \quad ,$$

we obtain

$$t_{90\%} = -\tau_F \ln(1 - 0.9) = 5.64 \mu\text{s} \quad .$$

#### I.11.16.4 EXERCISE 4: $\pi$ -MODE STRUCTURES

1. The shunt impedance of a multi-cell system is approximately  $N$  time the shunt impedance of the single cell

$$R_{TOT} = N \cdot R_{cell} = 24 \text{ M}\Omega \quad .$$

2. Using the above relation

$$V_{acc} = \sqrt{R_{TOT} P_{diss}} = 4.9 \text{ MV} \quad .$$

3. The average accelerating field is simply given by the total voltage divided by the structure length

$$E_{acc} = \frac{V_{acc}}{L_{cell} N} = 4.08 \text{ MV/m} \quad .$$

4. For a  $\pi$ -mode structure the distance between the centers of two adjacent cells is given by

$$d = \frac{\beta c}{2 f_{RF}} = \frac{\beta \lambda_{RF}}{2} \quad ,$$

and with

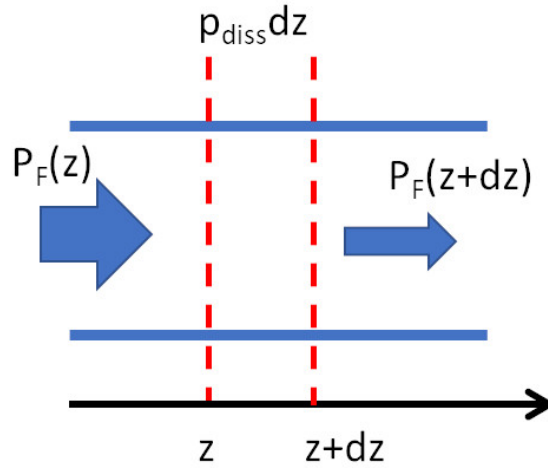
$$\lambda_{RF} = \frac{c}{f_{RF}} = 0.7495 \text{ m} \quad .$$

we obtain

$$\beta_{in} = 2 \frac{L_{cell}}{\lambda_{RF}} = 0.4 \quad ,$$

#### I.11.16.5 EXERCISE 5: TW STRUCTURES PARAMETERS

1. If we consider a generic section of a TW structure, as given in the figure below



we have that

$$\begin{aligned}
 P_F(z + dz) &= P_F(z) - p_{\text{diss}} dz \\
 P_F(z + dz) - P_F(z) &= -p_{\text{diss}} dz \\
 dP_F &= -p_{\text{diss}} dz \quad ,
 \end{aligned}$$

with

$$\alpha = \frac{p_{\text{diss}}}{2 P_F} \quad ,$$

it yields

$$\begin{aligned}
 \frac{dP_F}{dz} &= -2 \alpha P_F \\
 \frac{1}{P_F} \frac{dP_F}{dz} &= -2 \alpha \quad .
 \end{aligned}$$

Integrating and assuming  $P_F(0) = P_{\text{in}}$

$$P_F(z) = P_{\text{in}} e^{-2\alpha z} \quad .$$

2. Let us write some relations that will be useful for the demonstration

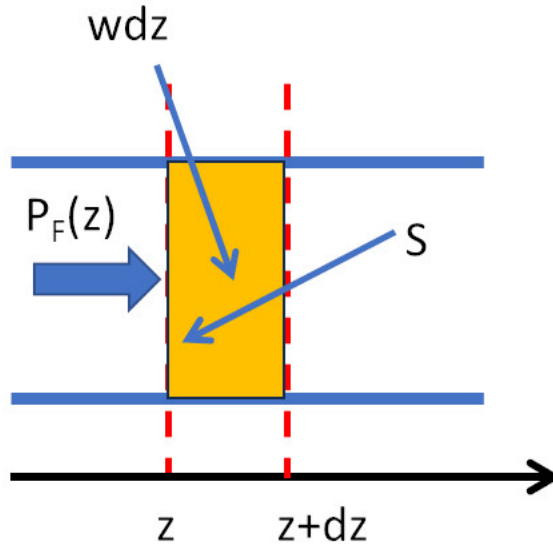
$$r = \frac{\hat{E}_{\text{acc}}^2}{p_{\text{diss}}} \quad \alpha = \frac{p_{\text{diss}}}{2 P_F} \quad P_F(z) = P_{\text{in}} e^{-2\alpha z} \quad ,$$

$$\hat{E}_{\text{acc}}(z) = \sqrt{r p_{\text{diss}}} = \sqrt{2 \alpha r P_F(z)} = \sqrt{2 \alpha r P_{\text{in}}} e^{-\alpha z} = E_{\text{in}} e^{-\alpha z} \quad ,$$

3.

$$V_{\text{acc}} = \int_0^L E_{\text{in}} e^{-\alpha z} dz = E_{\text{in}} \frac{1 - e^{-\alpha L}}{\alpha} \quad .$$

4. Let us consider a generic section of the TW structure. The stored energy is propagating, by definition, at the group velocity  $v_g$ . In a time  $dt$  the stored energy that flows through the section  $S$  (given



by  $w dz$ ) is exactly equal to the power flow  $P_F$  times  $dt$  and then

$$w dz = P_F(z) dt \Rightarrow \frac{dz}{dt} = v_g = \frac{P_F}{w} .$$

#### I.11.16.6 EXERCISE 6: TW STRUCTURES

1.

$$L = 3 \Rightarrow t_F = \frac{L}{v_g} = 909.7 \text{ ns} .$$

2.

$$V_{\text{acc}} = \int_0^L E_{\text{in}} e^{-\alpha z} dz = E_{\text{in}} \frac{1 - e^{-\alpha L}}{\alpha} = 45 \text{ MV} .$$

3.

$$E_{\text{acc}} = \frac{V_{\text{acc}}}{L} = 15 \text{ MV/m} .$$

4.

$$r = \frac{\hat{E}_{\text{acc}}^2}{p_{\text{diss}}} = 56.5 \text{ M}\Omega/\text{m} .$$

**I.11.16.7 EXERCISE 7:  $\pi$ -MODE STRUCTURES AND DUTY CYCLE**

1.

$$d = \frac{\beta_c}{2 f_{\text{RF}}} = \frac{\beta \lambda_{\text{RF}}}{2} = 7.5 \text{ cm} \quad .$$

2.

$$R_{\text{TOT}} = N R = 9 \text{ M}\Omega \quad \Rightarrow \quad P_{\text{diss}} = \frac{V_{\text{acc}}^2}{R_{\text{TOT}}} = 11.1 \text{ MW} \quad .$$

3.

$$L_{\text{TOT}} = dN = 67.4 \text{ cm} \quad \Rightarrow \quad E_{\text{acc}} = \frac{V_{\text{acc}}}{L_{\text{TOT}}} = 14.8 \text{ MV/m} \quad .$$

4.

$$\text{DC} = \frac{T_{\text{imp}}}{T_{\text{period}}} = \frac{410^{-6}}{0.01} = 4 \cdot 10^{-4} (0.04\%) \quad .$$

**Acknowledgements**

Several pictures, schemes, images and plots have been taken from papers and presentations reported in the references: I would like to acknowledge all the authors.



## Appendices

### Appendix I: SW field as a sum of two counter-propagating TW waves

In a multi-cell SW structure, the accelerating field can be generally expressed as

$$E_z = E_{\text{RF}}(z) \cos(\omega_{\text{RF}}t). \quad (\text{A1})$$

The spacial form factor  $E_{\text{RF}}(z)$  can be written in a simplified form as

$$E_z = \underbrace{\hat{E}_{\text{RF}} \cos(k_z z)}_{E_{\text{RF}}(z)} \cos(\omega_{\text{RF}}t). \quad (\text{A2})$$

In order to have synchronism between the accelerating field and the particle of velocity  $v$ , and supposing that the velocity variation of the particle while traversing the structure is negligible,  $k_z$  has to satisfy the following relation

$$k_z = \frac{2\pi}{vT_{\text{RF}}} = \frac{2\pi}{\beta\lambda_{\text{RF}}} = \frac{\omega_{\text{RF}}}{v}. \quad (\text{A3})$$

The accelerating field seen by the particle on crest is then given by ( $t = z/v$ )

$$E_{z, \text{ seen by particle } z=vt} = \hat{E}_{\text{RF}} \cos(k_z z) \cos\left(\omega_{\text{RF}} \frac{z}{v}\right) = \hat{E}_{\text{RF}} \cos^2(k_z z) = \frac{\hat{E}_{\text{RF}}}{2} + \frac{\hat{E}_{\text{RF}}}{2} \cos(2k_z z). \quad (\text{A4})$$

On the other hand, the SW can be written, with some math, as the sum of two TWs in the form

$$E_z = \hat{E}_{\text{RF}} \cos(k_z z) \cos(\omega_{\text{RF}}t) = \frac{\hat{E}_{\text{RF}}}{2} \cos(\omega_{\text{RF}}t - k_z z) + \frac{\hat{E}_{\text{RF}}}{2} \cos(\omega_{\text{RF}}t + k_z z). \quad (\text{A5})$$

Substituting in this last expression  $t = z/v$  we obtain the same expression (A4). In conclusion, the SW field can be “seen” as the superposition of two counter-propagating TW waves. The co-propagating one is that gives the net acceleration  $E_z = \hat{E}_{\text{RF}}/2$ , while the other one (back propagating) does not contribute to the acceleration but generates an oscillating term with no net acceleration effect.

### Appendix II: Large longitudinal oscillations and separatrix

To study the longitudinal dynamics at large oscillations, we have to consider the non-linear system of differential equation as given in Eq. I.11.54 in the adiabatic acceleration case. Eq.I.11.54 also works for  $\phi$  in the form

$$\frac{d^2\phi}{dz^2} = -\frac{\omega_{\text{RF}}q\hat{E}_{\text{acc}}}{cE_0\beta_s^3\gamma_s^3} [\cos\phi - \cos\phi_s] = F(\phi). \quad (\text{A6})$$

The function  $F(\phi)$  acts as a non linear restoring force. We can then write

$$\frac{d}{dz} \left( \frac{d\phi}{dz} \right)^2 = 2 \frac{d\phi}{dz} \frac{d^2\phi}{dz^2} = 2 \frac{d\phi}{dz} \cdot F = 2 \frac{d}{dz} \int_0^\phi F d\phi. \quad (\text{A7a})$$

Therefore

$$\frac{d}{dz} \left[ \left( \frac{d\phi}{dz} \right)^2 - 2 \int_0^\phi F d\phi \right] = 0, \quad (\text{A7b})$$

thus

$$\frac{1}{2} \left( \frac{d\phi}{dz} \right)^2 - \int_0^\phi F d\phi = \text{const}, \quad (\text{A7c})$$

and finally

$$\frac{1}{2} \frac{\omega_{\text{RF}}}{c E_0 \beta_s^3 \gamma_s^3} w^2 + q \hat{E}_{\text{acc}} [\sin \phi - \phi \cos \phi_s] = H. \quad (\text{A7d})$$

That is Eq. I.11.58. To find the  $H$  value for the separatrix we have to remember that for  $\phi = -\phi_s$ ,  $w = 0$  and then we have  $q \hat{E}_{\text{acc}} [-\sin \phi_s + \phi_s \cos \phi_s] = H_{\text{sep}}$  and then substituting in Eq. A7d we obtain the equation of the separatrix

$$\frac{1}{2} \frac{\omega_{\text{RF}}}{c E_0 \beta_s^3 \gamma_s^3} w^2 + q \hat{E}_{\text{acc}} [\sin \phi + \sin \phi_s - (\phi + \phi_s) \cos \phi_s] = 0. \quad (\text{A8})$$

For small amplitude oscillations around the synchronous phase, Eq. A7d becomes (also considering that  $\phi = \phi_s + \varphi$ )

$$\frac{1}{2} \frac{\omega_{\text{RF}}}{c E_0 \beta_s^3 \gamma_s^3} w^2 + q \hat{E}_{\text{acc}} \left[ \cos(\phi_s) \varphi - \frac{1}{2} \sin \phi_s \varphi^2 - (\phi_s + \varphi) \cos \phi_s \right] = H \quad (\text{A9a})$$

and therefore

$$\frac{1}{2} \frac{\omega_{\text{RF}}}{c E_0 \beta_s^3 \gamma_s^3} w^2 - \frac{1}{2} q \hat{E}_{\text{acc}} \sin \phi_s \varphi^2 = H. \quad (\text{A9b})$$

### Appendix III: Transverse Lorentz force in a multi-cell SW structure

For a multi-cell structure let us suppose that the field can be written as Eq. A2. According to Eq. I.11.74, the Lorentz force due to the transverse electric and magnetic field are then given by

$$\begin{aligned} F_{r,E} &= -q \frac{r}{2} \frac{\partial E_{\text{RF}}(z)}{\partial z} \cos \left( \omega_{\text{RF}} \frac{z}{\beta c} + \phi_{\text{inj}} \right) = q \frac{r}{2} \hat{E}_{\text{RF}} \sin(kz) \cos \left( \omega_{\text{RF}} \frac{z}{\beta c} + \phi_{\text{inj}} \right) \\ &= q \frac{r}{2} \frac{\omega_{\text{RF}}}{\beta c} \hat{E}_{\text{RF}} \sin \left( \omega_{\text{RF}} \frac{z}{\beta c} \right) \cos \left( \omega_{\text{RF}} \frac{z}{\beta c} + \phi_{\text{inj}} \right) = q \frac{r}{4} \frac{\omega_{\text{RF}}}{\beta c} \hat{E}_{\text{RF}} \left[ \sin(-\varphi_s) + \cos \left( 2\omega_{\text{RF}} \frac{z}{\beta c} + \phi_{\text{inj}} \right) \right] \end{aligned} \quad (\text{A10})$$

and

$$F_{r,B} = q \frac{r}{2} \omega_{\text{RF}} \frac{\beta}{c} \hat{E}_{\text{RF}} \cos(kz) \sin \left( \omega_{\text{RF}} \frac{z}{\beta c} + \phi_{\text{inj}} \right) = q \frac{r}{4} \omega_{\text{RF}} \frac{\beta}{c} \hat{E}_{\text{RF}} \left[ \sin(\varphi_s) + \cos \left( 2\omega_{\text{RF}} \frac{z}{\beta c} + \phi_{\text{inj}} \right) \right]. \quad (\text{A11})$$

And then adding the two terms

$$F_{r,E} + F_{r,B} = q \frac{r}{2} \frac{\pi \hat{E}_{\text{RF}}}{\lambda_{\text{RF}} \beta \gamma^2} \sin(-\phi_{\text{inj}}) + q \frac{r}{2} \frac{\pi \hat{E}_{\text{RF}}}{\lambda_{\text{RF}}} \left( \frac{\beta^2 + 1}{\beta} \right) \cos \left( 2\omega_{\text{RF}} \frac{z}{\beta c} + \phi_{\text{inj}} \right). \quad (\text{A12})$$

The first term of the equation is a positive defocusing term representing the rf force due to the synchronous harmonic (forward wave) while the second term is zero on average and is given by the non-synchronous harmonic (backward wave). In electron linacs this gives a positive focus as calculated in Appendix IV

#### Appendix IV: ponderomotive force and focusing term due to the non-synchronous RF harmonics

Equation A12 clearly shows that the transverse rf force due to the non-synchronous rf harmonic has, apparently, a zero average net effect. In general, we can have several non-synchronous harmonics due to the correct Fourier content of the real accelerating field profile also in the case of TW fields but the intensity of this harmonics is much stronger in SW cavities due to the presence of the backward wave. In a very generic form we can write, for the transverse motion, an equation of the type

$$\ddot{r} = \frac{1}{\gamma m_0} r \sum_n a_n \cos(n\omega_{\text{RF}}t), \quad (\text{A13})$$

where the dot represents the derivative with respect to time. Let us consider the contribution of the single harmonics with a generic amplitude  $A$

$$\ddot{r} = Ar \cos(n\omega_{\text{RF}}t). \quad (\text{A14})$$

The solution of this equation in its general form is not trivial and the hypothesis we can do to solve it is that the solution is of the type

$$r \cong r_s(t) + r_f(t), \quad (\text{A15})$$

where  $r_s$  represents a slow drift motion and  $r_f$  a fast oscillation. The equation becomes

$$\ddot{r}_s + \ddot{r}_f = [A(r_s + r_f)] \cos(n\omega_{\text{RF}}t). \quad (\text{A16})$$

Assuming  $\ddot{r}_s \ll \ddot{r}_f$  and  $r_s \gg r_f$  we have

$$\ddot{r}_f = Ar_s \cos(n\omega_{\text{RF}}t). \quad (\text{A17})$$

If we assume that on the time scale on which  $r_f$  oscillates  $r_s$  is essentially constant the equation can be integrated to get

$$r_f = -\frac{Ar_s}{(n\omega_{\text{RF}})^2} \cos(n\omega_{\text{RF}}t). \quad (\text{A18})$$

Substituting Eq. A18 in Eq. A16 and averaging over one period we have

$$\ddot{r}_s = -\frac{A^2}{2(n\omega_{\text{RF}})^2}r_s. \quad (\text{A19})$$

That represents the equation of motion with a restoring force with an average intensity equal to

$$\bar{F}_r = -\frac{A^2}{2(n\omega_{\text{RF}})^2}\gamma m_0 r_s. \quad (\text{A20})$$

If we consider the expression of the transverse force in the SW case, as expressed by Eq. A12 it is enough to substitute in Eq. A20 the quantities  $n = 2$  and

$$A = q \frac{1}{2} \frac{\pi \hat{E}_{\text{RF}}}{\lambda_{\text{RF}} \gamma m_0} \left( \frac{\beta^2 + 1}{\beta} \right),$$

thus obtaining, if we consider  $\beta = 1$

$$\bar{F}_r = -rq \frac{\hat{E}_{\text{RF}}^2}{32\gamma m_0 c^2 / e}. \quad (\text{A21})$$

Equation A21 has a similar expression as Eq. I.11.76.

## References

- [1] T. Wangler, RF Linear Accelerators (Wiley, New York, 1998), [doi:10.1002/9783527618408](https://doi.org/10.1002/9783527618408).
- [2] P.M. Lapostolle and A.L. Septier, Linear Accelerators (North-Holland, Amsterdam, 1970).
- [3] A. Wambersie and R.A. Gahbauer, Medical applications of electron linear accelerators, CAS - CERN Accelerator School: Cyclotrons, Linacs and their applications, CERN 96-02, Geneva, 1994, [doi:10.5170/CERN-1996-002.229](https://doi.org/10.5170/CERN-1996-002.229).
- [4] K.H.W. Bethge, Non-medical applications of linacs, CAS - CERN Accelerator School: Cyclotrons, Linacs and their applications, CERN 96-02, Geneva, 1994, [doi:10.5170/CERN-1996-002.249](https://doi.org/10.5170/CERN-1996-002.249).
- [5] K.H.W. Bethge, Applications of ion linacs, CAS - CERN Accelerator School: Cyclotrons, Linacs and their applications, CERN 96-02, Geneva, 1994, [doi:10.5170/CERN-1996-002.259](https://doi.org/10.5170/CERN-1996-002.259).
- [6] I. Hofmann, Application of RF-linacs to heavy-ion fusion, CAS - CERN Accelerator School: Cyclotrons, Linacs and their applications, CERN 96-02, Geneva, 1994, [doi:10.5170/CERN-1996-002.267](https://doi.org/10.5170/CERN-1996-002.267).
- [7] H. Lengeler, Application of high intensity linacs to spallation sources, CAS - CERN Accelerator School: Cyclotrons, Linacs and their applications, CERN 96-02, Geneva, 1994, [doi:10.5170/CERN-1996-002.285](https://doi.org/10.5170/CERN-1996-002.285).
- [8] B.L. Doyle, F.D. McDaniel and R. W. Hamm, The Future of Industrial Accelerators and Applications, OSTI.
- [9] N. Pichoff, Introduction to RF linear accelerators, CAS - CERN Accelerator School: Intermediate Accelerator Physics, pp.105-128, 2003, [doi:10.5170/CERN-2006-002.105](https://doi.org/10.5170/CERN-2006-002.105).
- [10] D. Alesini, LINAC, proc. of CAS - CERN Accelerator School 2019: Introduction to Accelerator Physics, 2021, [doi:10.48550/arXiv.2103.16500](https://doi.org/10.48550/arXiv.2103.16500).
- [11] J.D. Cockcroft and E.T.S. Walton, "Experiments with high velocity ions", Proc. Royal Soc., Series A 136 (1932), 619–30.
- [12] G. Ising, Arkiv för Matematik, Astronomi och Fysik, 18 (1924), 1–4.
- [13] R. Widerøe, Arch.für Elektrotechnik, 21 (1928), 387–406.
- [14] Bryant, P J, A brief history and review of accelerators, CAS - CERN Accelerator School: 5th General Accelerator Physics Course, pp.1-16, 1994, [doi:10.5170/CERN-1994-001.1](https://doi.org/10.5170/CERN-1994-001.1).
- [15] E. Jensen, Cavity basics, in Proceedings of the CAS–CERN Accelerator School: RF for Accelerators, Ebeltoft, Denmark, 8–17 June 2010, CERN-2011-007 (CERN, Geneva, 2010) pp. 259–275, [doi:10.48550/arXiv.1201.3202](https://doi.org/10.48550/arXiv.1201.3202).
- [16] F. Gerigk, Cavity types, in Proceedings of the CAS–CERN Accelerator School: RF for Accelerators, Ebeltoft, Denmark, 8–17 June 2010, CERN-2011-007 (CERN, Geneva, 2010), pp. 277–298, [doi:10.48550/arXiv.1111.4897](https://doi.org/10.48550/arXiv.1111.4897).
- [17] L. Alvarez, The design of a proton linear accelerator, Phys. Rev. 70 (1946) 799.
- [18] M. Vretenar, J. Vollaire et al., Linac4 design report, CERN Yellow Reports: Monographs, CERN-2020-006, [doi:10.23731/CYRM-2020-006](https://doi.org/10.23731/CYRM-2020-006).

- [19] D. Alesini, Power coupling, in Proceedings of the CAS–CERN Accelerator School: RF for Accelerators, Ebeltoft, Denmark, 8–17 June 2010, CERN-2011-007 (CERN, Geneva, 2010), pp.125–147, [doi:10.48550/arXiv.1112.3201](https://doi.org/10.48550/arXiv.1112.3201).
- [20] D. Alesini, Linear Accelerator Technology, Proceedings of the CAS-CERN Accelerator School on Free Electron Lasers and Energy Recovery Linacs, Vol. 1 (2018), [doi:10.23730/CYRSP-2018-001](https://doi.org/10.23730/CYRSP-2018-001).
- [21] DESY, Technical Design Report (TDR) of the European XFEL, 2007, [http://xfel.desy.de/technical\\_information/tdr/tdr/](http://xfel.desy.de/technical_information/tdr/tdr/).
- [22] B. Aune et al., Phys. Rev. ST Accel. Beams 3(9) (2000) 092001, [doi:10.1103/PhysRevSTAB.3.092001](https://doi.org/10.1103/PhysRevSTAB.3.092001).
- [23] S. Henderson, et al., The Spallation Neutron Source accelerator system design, Nuclear Instruments and Methods in Physics Research Section A, Volume 763, 2014, Pages 610-673, [doi:10.1016/j.nima.2014.03.067](https://doi.org/10.1016/j.nima.2014.03.067).
- [24] R.E. Collin, Foundations for Microwave Engineering, 2nd ed. (McGraw-Hill, Singapore, 1992).
- [25] R.B. Neal, The Stanford Two-Mile Accelerator (Benjamin, New York, 1968).
- [26] T. Garvey, The SwissFEL Linac (2014) [www-pnp.physics.ox.ac.uk/jaiweb/slides/2014\\_Garvey.pdf](http://www-pnp.physics.ox.ac.uk/jaiweb/slides/2014_Garvey.pdf).
- [27] R. Zennaro et al., Measurements and high power test of the first C-band accelerating structure for SwissFEL, Proc. LINAC2014, Geneva, Switzerland, (Jacow, CERN, Geneva, 2014), p. 333.
- [28] J.-Y. Raguin and M. Bopp, The Swiss FEL C-band accelerating structure: RF design and thermal analysis, Proc. LINAC2012, Tel-Aviv, Israel, (Jacow, CERN, Geneva, 2013), p. 501.
- [29] J. Wang, PhD thesis, SLAC Report 339, <https://www.slac.stanford.edu/pubs/slacreports/reports08/slac-r-339.pdf>, 1989.
- [30] T. Inagaki et al., Phys. Rev. ST Accel. Beams 17(8) (2014) 080702, [doi:10.1103/PhysRevSTAB.17.080702](https://doi.org/10.1103/PhysRevSTAB.17.080702).
- [31] K. Okihira, Mass production report of C-band choke mode accelerating structure and RF pulse compressor, Proc. IPAC2011, San Sebastián, Spain, 2011, (EPS-AG, Geneva, 2011), p. 668.
- [32] R. Parodi, Multipacting, in Proceedings of the CAS–CERN Accelerator School: RF for Accelerators, Ebeltoft, Denmark, 8–17 June 2010, CERN-2011-007 (CERN, Geneva, 2010), pp.447–458, [doi:10.5170/CERN-2011-007](https://doi.org/10.5170/CERN-2011-007).
- [33] D.C. Mattis and J. Bardeen, Phys. Rev. 111(2) (1958) 412, [doi:10.1103/PhysRev.111.412](https://doi.org/10.1103/PhysRev.111.412).
- [34] H. Padamsee. RF Superconductivity: Science, Technology, and Applications (Wiley-VCH, Weinheim, 2009), [doi:10.1002/9783527627172](https://doi.org/10.1002/9783527627172).
- [35] H. Padamsee, J. Knobloch, and T. Hays. RF Superconductivity for Accelerators (Wiley, New York, 1998).
- [36] H. Safa, SuRFace effects in SCRF cavity, in Proceedings of the CAS–CERN Superconductivity and Cryogenics for Accelerators and Detectors, Erice, 2002, CERN 2004-008 (CERN, Geneva, 2004), p. 196, [doi:10.5170/CERN-2004-008](https://doi.org/10.5170/CERN-2004-008).
- [37] G. Bisoffi, Superconducting cavities, in Proceedings of the CAS School on Radiofrequency Engineering, CERN 2005-003 (CERN, Geneva, 2005), p. 315, [doi:10.5170/CERN-2005-003.315](https://doi.org/10.5170/CERN-2005-003.315).

- [38] S. Belomestnykh, Principles of RF superconductivity, lecture at USPAS 2013, Durham, NC, 2013, <http://uspas.fnal.gov/materials/materials-table.shtml>.
- [39] G. Ciovati, Cavity fabrication, lecture at USPAS 2015, [http://uspas.fnal.gov/materials/15Rutgers/Cavity\\_Fabrication.pdf](http://uspas.fnal.gov/materials/15Rutgers/Cavity_Fabrication.pdf).
- [40] D. Proch, RF cavity fabrication, in Proceedings of the CAS–CERN Accelerator School, Superconductivity and Cryogenics for Accelerators and Detectors, Erice, 2002, CERN 2004-008 (CERN, Geneva, 2004), p. 214, [doi:10.5170/CERN-2004-008.214](https://doi.org/10.5170/CERN-2004-008.214).
- [41] J. Le Duff, Dynamics and Acceleration in Linear Structures, CAS-CERN Accelerator School: 5th general accelerator physics course, Jyväskylä, CERN 94-01, Finland, 7-18 Sep 1992, [doi:10.5170/CERN-1994-001.253](https://doi.org/10.5170/CERN-1994-001.253).
- [42] M. Ferrario et al., Experimental Demonstration of Emittance Compensation with Velocity Bunching, Phys. Rev. Lett. 104, 054801, 2010.
- [43] J.B. Rosenzweig and L. Serafini, "Transverse Particle Motion In Radio-Frequency Linear Accelerators", Physical Review E 49, 1499 (1994).
- [44] S. Heifets, G. Stupakov, and S. Krinsky, Phys. Rev. STAccel. Beams5, 064401 (2002).
- [45] Z. Huang and K. J. Kim, Phys. Rev. ST Accel. Beams5, 074401 (2002).
- [46] I. M. Kapchinskiy and V.A. Tepliakov, Prib. Tekh. Eksp. 2, 19-22 (1970).
- [47] M. Weiss, Radio Frequency Quadrupole, CAS: Fifth advanced accelerator physics course, CERN 95-06, 1995, [doi:10.5170/CERN-1995-006.959](https://doi.org/10.5170/CERN-1995-006.959).
- [48] H. Padamsee, Design Topics for Superconducting RF Cavities and Ancillaries, contribution to the CAS-CERN Accelerator School: Superconductivity for Accelerators, Erice, Italy, 24 April - 4 May 2013, 2015, [doi:10.5170/CERN-2014-005.141](https://doi.org/10.5170/CERN-2014-005.141).